**U.S. DEPARTMENT OF THE INTERIOR**
**U.S. GEOLOGICAL SURVEY**

# Application of Heat Flow Equation to Analyses of Bottom Simulating Reflections

by
Myung W. Lee[1]

Open-File Report 95-262



1U.S. Geological Survey, Box 25046, Denver Federal Center, Denver, CO 80225

# Table of Contents



# Table of Figures



# Table of Tables

## ABSTRACT

The hydrate stability field is sensitive to the pressure and temperature in the earth, so the depth to a bottom simulating reflector (BSR), which occurs at the phase boundary, can be used to determine regional conductive heat flow. The inferred heat flow values estimated from the BSR depths in the recent slide on the Carolina Continental Rise, southeastern United States, indicate that the heat flow values in the slide area are significantly different from those in the adjacent undisturbed area. This difference in the heat flow values could be caused by a local perturbation of temperature in the sediments either by a local heat source or advective fluid flow.

In order to estimate the amount of heat source or advective fluid flow accountable for the difference in heat flow values, the temperature distribution in the earth by a local heat perturbation is required and this temperature perturbation are computed by one- and two-dimensional finite difference equations for inhomogeneous heat flow equations. Analytic solutions for homogeneous one-dimensional heat flow equations are derived in order to examine the numerical results and analyze the time required to reach the steady-state condition.

The depth-dependent thermal gradients observed at the Deep Sea Drilling Project (DSDP) well 533 could be explained by introducing a local heat source located between 40 m and 140 m in depth with a magnitude of 200 $\mu W m^{-3}$. However, the heat source model is not unique, so the heat source model should be considered as one of the possible solutions explaining the depth-dependent thermal gradients at DSDP 533 hole.


## INTRODUCTION

Natural-gas hydrates are stable at the temperature and pressure conditions that exist near and beneath the sea floor in the world's ocean where water depths exceed 300 to 500 m (Kvenvolden, 1993). Temperature increases downward through the sediments along the geothermal gradient, and although pressure also increases, the conditions become ultimately too hot for hydrate to exist. The lower boundary of gas hydrate phase stability represents a contact between hydrate-bearing sediments and those containing water plus, commonly free gas in their pores. This contact frequently manifest itself as bottom simulating reflectors (BSRs) in seismic profiles (Markl and others, 1970; Tucholke and others, 1977; Shipley and others, 1979)

Because the temperature and pressure conditions at the phase boundary are well known from laboratory measurements (Sloan, 1990), they can be used to determine the temperature at the BSR level. From this in-situ temperature, with other pertinent parameters, heat flow can be inferred from the measured BSR depth. Uyeda and others (1982) estimated the heat flow from the BSR depths at the Nankai Trough and compared these values with the actual heat flow measurements. They concluded that because of a few uncertain factors such as the thermal conductivity and interval velocity, the accuracy of the estimated values is not very high, but the values are consistent with those measured by conventional means.

An analysis of BSRs at the Gulf of Oman indicates that a heat flow profile derived from the BSR depths does not show the expected landward decrease of BSR depths as the sediment pile thickens (Minshull and White, 1989). They attributed this anomaly to the advective heat flow within the prism. Similarly Davis and Hyndman (1990) performed detailed analysis of heat flow measurements and BSRs at the Northern Cascadia accretionary prism. They observed that measured heat flow values are as much as 30 % higher than inferred heat flow values from the BSR depths and they explained this discrepancy by the advective heat transport resulting from the dewatering of the prism sediments.

In order to quantify the magnitude of a local heat source or an advective fluid flow that influences the BSR depths, temperature in the sediments must be known accurately. In cases where the material properties of the sediments, such as the thermal conductivity, are dependent on the location in the sediments, a numerical method is required to solve the heat flow equation. Sawyer (1982) used a two-dimensional finite difference equation in his study of thermal evolution of the northern United States Atlantic continental margin. Hutchison (1988) used one-dimensional a finite difference equation in order to predict thermal parameters and material advection rates for an evolving sediment/basement system.

In this paper one- and two-dimensional finite difference equations for inhomogeneous heat flow including a heat source term and an advective fluid flow term are solved in order to derive temperature distribution in the sediments. Two boundary conditions, a constant temperature and a constant heat flux, are utilized in the difference equation. The solutions of the difference equation are used to predict the BSR depths and the amount of surface heat flow contributed by the local heat perturbation.


## ACKNOWLEDGEMENTS

I like to thank William Dillon, Timothy Collett and Colin Williams for their very helpful and constructive comments.


## HEAT FLOW EQUATION

An inhomogeneous equation for the temperature within the sediment can be described by the following heat flow equation (Hutchison, 1985).

$$\rho C\frac{\partial T}{\partial t}+\rho_o C_o[\nabla\cdot\phi\mathbf{F}T]+\rho C[\nabla\cdot(1-\phi)\mathbf{S}T] \quad =\nabla\cdot(k\nabla T) \quad + \quad H \qquad (1)$$

where $\rho$ is the density of the sediment, C is the specific heat of the sediment at the constant pressure, $\rho_o$ is the fluid density and $C_o$ is the specific heat of the fluid at constant pressure, k is the thermal conductivity of the sediment, **F** is the fluid velocity, **S** is the sediment particle velocity, $\phi$ is the porosity of the sediment, H is the rate of internal heat generation and T is the temperature.

In the two-dimensional orthogonal cartesian coordinate system, Equation (1) can be written as:

$$\frac{\partial}{\partial x}\left(k\frac{\partial T}{\partial x}\right)+\frac{\partial}{\partial z}\left(k\frac{\partial T}{\partial z}\right)-\beta^o\frac{\partial}{\partial x}(\phi F^x T)-\beta\frac{\partial}{\partial x}((1-\phi)S^x T)-\beta^o\frac{\partial}{\partial z}(\phi F^z T)-\beta\frac{\partial}{\partial z}((1-\phi)S^z T)$$

$$=\beta\frac{\partial T}{\partial t}-H, \qquad (2)$$

$$\text{with} \quad \beta=\rho C, \quad \beta^o=\rho_o C_o.$$

The superscripts x and z in Equation (2) represent the directions of velocity components.

The solution of Equation (2) is very complex because of the spatial dependence of the coefficients. Sclater and Francheteau(1970) analytically solved a similar but a simpler equation under the assumption of the steady-state condition with the constant thermal conductivity, density and specific heat, but included a heat source and an advective term in the solution. In

order to solve Equation (2) without any further assumptions, a numerical approach using a finite difference approximation is attempted. Both non-steady and steady state equations are considered here.

## NON-STEADY STATE SOLUTION

### A) Two-Dimensional Solution

Using a central difference scheme for the spatial derivative and a forward difference for the time derivative, the derivatives in Equation (2) can be approximated by the following difference equations.

Let $T(x,z,t) = T(i\Delta x, j\Delta z, n\Delta t) = T_{i,j}^{n}$. Then

$$\frac{\partial T}{\partial t} = \frac{T_{i,j}^{n+1} - T_{i,j}^{n}}{\Delta t},$$

$$\frac{\partial^2 T}{\partial x^2} = \frac{T_{i+1,j}^{n} - 2T_{i,j}^{n} + T_{i-1,j}^{n}}{\Delta x^2},$$

$$\beta^{o} \frac{\partial}{\partial x}(\phi FT) = \beta_{i,j}^{o} \frac{\phi_{i+1} F_{i+1,j}^{n} T_{i+1,j}^{n} - \phi_{i-1} F_{i-1,j}^{n} T_{i-1,j}^{n}}{2\Delta x}. \tag{3}$$

In Equation (3), $\Delta x, \Delta z$ and $\Delta t$ are the horizontal grid spacing, the vertical grid spacing and the time increment respectively. Using Equations (2) and (3), the two-dimensional finite difference approximation for the heat flow equation can be written as:

$$\begin{aligned}
T_{i,j}^{n+1} = {} & \frac{\Delta t}{4\beta_{i,j}\Delta x^2}\{(k_{i+1,j} + 4k_{i,j} - k_{i-1,j})T_{i+1,j}^{n} - 8k_{i,j}T_{i,j}^{n} + (-k_{i-1,j} + 4k_{i,j} + k_{i-1,j})T_{i-1,j}^{n}\} \\
& + \frac{\Delta t}{4\beta_{i,j}\Delta z^2}\{(k_{i,j+1} + 4k_{i,j} - k_{i,j-1})T_{i,j+1}^{n} - 8k_{i,j}T_{i,j}^{n} + (-k_{i,j+1} + 4k_{i,j} + k_{i,j-1})T_{i-1,j}^{n}\} \\
& - \frac{\Delta t \beta_{i,j}^{o}}{2\Delta x \beta_{i,j}}(\phi_{i+1,j} F_{i+1,j}^{x,n} T_{i+1,j}^{n} - \phi_{i-1,j} F_{i-1,j}^{x,n} T_{i-1,j}^{n}) \\
& - \frac{\Delta t \beta_{i,j}^{o}}{2\Delta z \beta_{i,j}}(\phi_{i,j+1} F_{i,j+1}^{z,n} T_{i,j+1}^{n} - \phi_{i,j-1} F_{i,j-1}^{z,n} T_{i,j-1}^{n}) \\
& - \frac{\Delta t}{2\Delta x}\{(1-\phi_{i+1,j}) S_{j+1,j}^{x,n} T_{i+1,j}^{n} - (1-\phi_{i-1,j}) S_{i-1,j}^{x,n} T_{i-1,j}^{n}\} \\
& - \frac{\Delta t}{2\Delta z}\{(1-\phi_{i,j+1}) S_{i,j+1}^{z,n} T_{i,j+1}^{n} - (1-\phi_{i,j-1}) S_{i,j-1}^{z,n} T_{i,j-1}^{n}\} \\
& + \frac{\Delta t}{\beta_{i,j}} H_{i,j}^{n} + T_{i,j}^{n}
\end{aligned} \tag{4}$$

Let's consider a rectangular region with boundary (i = 1 and I : j = 1 and J). The appropriate boundary conditions are:
a) At the top of the region (j = 1 for all i) - the constant temperature:

$$T^n_{i,1} = T_o. \tag{5a}$$

b) At the bottom of the region (j = J for all i)- the constant heat flux or the constant temperature. For the constant heat flux,

$$T^n_{i,J} = T^n_{i,J-1} + \frac{Q_B \Delta z}{k_J}, \tag{5b}$$

where $Q_B$ is the heat flux at the basement or heat flux at depth which can be considered as constant. For a constant temperature, the boundary condition is the same form as that at the top of the model.
c) At the right and left edge (i = 1 or I for all j) - no lateral heat transfer:

$$T^n_{1,j} = T^n_{2,j} \qquad \text{and} \qquad T^n_{I,j} = T^n_{I-1,j}. \tag{5c}$$

Other kinds of boundary conditions can be easily implemented in the framework of a finite difference approximation. For example, let's assume that the boundary temperature is changing with time and it is known. Then the boundary condition in Equation (5a) can be written as

$$T^n_{i,1} = T^n_o.$$

The initial condition for the temperature inside the region can be computed with initial heat flux Q with $T_o$. Other initial conditions can be easily implemented in the finite difference formulation.

Equation (4) implies that if the temperature at n-step, the fluid and solid velocity, and other physical properties are known throughout the model, the temperature at n+1 step can be computed by Equation (4) with boundary conditions shown in Equation (5). For the homogeneous medium without a source or an advective term, the computation of temperature at any point, which serves either as a boundary condition or initial condition, is easy. However for the depth-dependent thermal conductivity, initial temperature is not simple to compute. Thus for the initial temperature distribution for a model having depth-dependent conductivities, I used the solution of the finite difference equation with constant flux at the lower boundary without a source or an advective term.

The solution of Equation (4) makes sense only if the solution is stable. The general stability condition for Equation (4) is very complicated. So it is assumed that the stability condition for the explicit scheme shown in Equation (4) is the same as that of a simpler difference equation. The simpler equation is the heat flow equation without a heat source term or an advective flow term under the assumption of constant parameters. If the stability condition for the simpler equation does not work for the general equation, we simply decrease the previous sampling interval ($\Delta t$) until a stability is reached. The simpler explicit difference scheme is stable, if the following condition for sampling interval is satisfied (Sawyer, 1982).

$$\Delta t \le \frac{\rho C}{2k}\left\{\frac{1}{\Delta x^2} + \frac{1}{\Delta z^2}\right\}^{-1}. \tag{6}$$

For the inhomogeneous media, we choose the minimum $\rho C$ and maximum k in Equation (6) to insure the stability condition.

For the following numerical examples in this paper, constant $\beta = 0.25 \times 10^7$ Cal/ (°C cm$^3$) and $\beta^o = 1.0 \times 10^7$ Cal/ (°C cm$^3$) instead of depth-dependent variables were used for the sake of convenience. It is assumed that the thermal conductivity depends only on the porosity of the sediment and the porosity is a function of depth only. For the depth-dependent thermal conductivity, a simple geometric mean of the conductivities of pore fluid (0.6 $Wm^{-1}K^{-1}$) and matrix (2.4 $Wm^{-1}K^{-1}$) (Sass and others, 1971) was applied. The porosity was computed assuming that the porosity exponentially decreases with depth (Hutchison, 1985); the porosity-depth relationship is given by $\phi = 0.65\,EXP(-z/1500)$. This porosity equation provides the thermal conductivity of 0.975 $Wm^{-1}K^{-1}$ at the surface and 1.31 $Wm^{-1}K^{-1}$ at the depth of 600 m.

Figure 1 shows a schematic diagram of a two-dimensional landslide model in which 200 m of sediment is assumed to have initially slid away and Figure 2 shows the temperature distribution (solid lines) and the average thermal gradient (dashed lines) at location A without a local heat source or an advective fluid flow during the first 20,000 years after the landslide. The average thermal gradient is defined here as the difference between the surface temperature and temperature at depth divided by the depth. The model was run with $\Delta x = \Delta z = 50\,m, \Delta t = 20$ years, $T_o = 2.4$°C with a constant flux boundary condition of $Q_B = 40$ mW/m$^2$ at the bottom of the model. Because of the cold water at the water bottom, the temperature in the medium will decreases as time progresses. At the depth of 400 m, the temperature dropped about 4°C in 20,000 years. The rate of temperature drop is inversely proportional to the elapsed time. The landslide is modeled after a recent slide on the Carolina Continental Rise.

**B) One-Dimensional Solution**

If the temperature and other parameters in Equation (1) depend only on the vertical direction (z-direction), Equation (4) can be simplified to the following one-dimensional equation retaining subscript j for the z-direction.

$$T_j^{n+1} = \frac{\Delta t}{4\beta_j \Delta z^2}\{(k_{j+1} + 4k_j - k_{j-1})T_{j+1}^n - 8k_j T_j^n + (-k_{j+1} + 4k_j + k_{j-1})T_{j-1}^n\}$$

$$- \frac{\Delta t \beta_j^o}{2\Delta z \beta_j}(\phi_{j+1} F_{j+1}^{z,n} T_{j+1}^n - \phi_{j-1} F_{j-1}^{z,n} T_{j-1}^n)$$

$$- \frac{\Delta t}{2\Delta z}\{(1-\phi_{j+1}) S_{j+1}^{z,n} T_{j+1}^n - (1-\phi_{j-1}) S_{j-1}^{z,n} T_{j-1}^n\}$$

$$+ \frac{\Delta t}{\beta_j} H_j^n + T_j^n \qquad (7)$$

Figure 3 shows one-dimensional examples of the temperature distribution for the first 20,000 years with a local heat source located between 40 m and 100 m in depth. The parameters for the constant thermal conductivity model (Figure 3a) are $T_o = 2.4$°C, H = 250 $\mu Wm^{-3}$, and Q = 40 mW/m$^2$ at the depth of 600 m. The parameters for the depth-dependent thermal conductivity model (Figure 3b) are $T_o = 2.4$°C, H = 200 $\mu Wm^{-3}$, and Q = 44 mW/m$^2$ at the depth of 600 m.

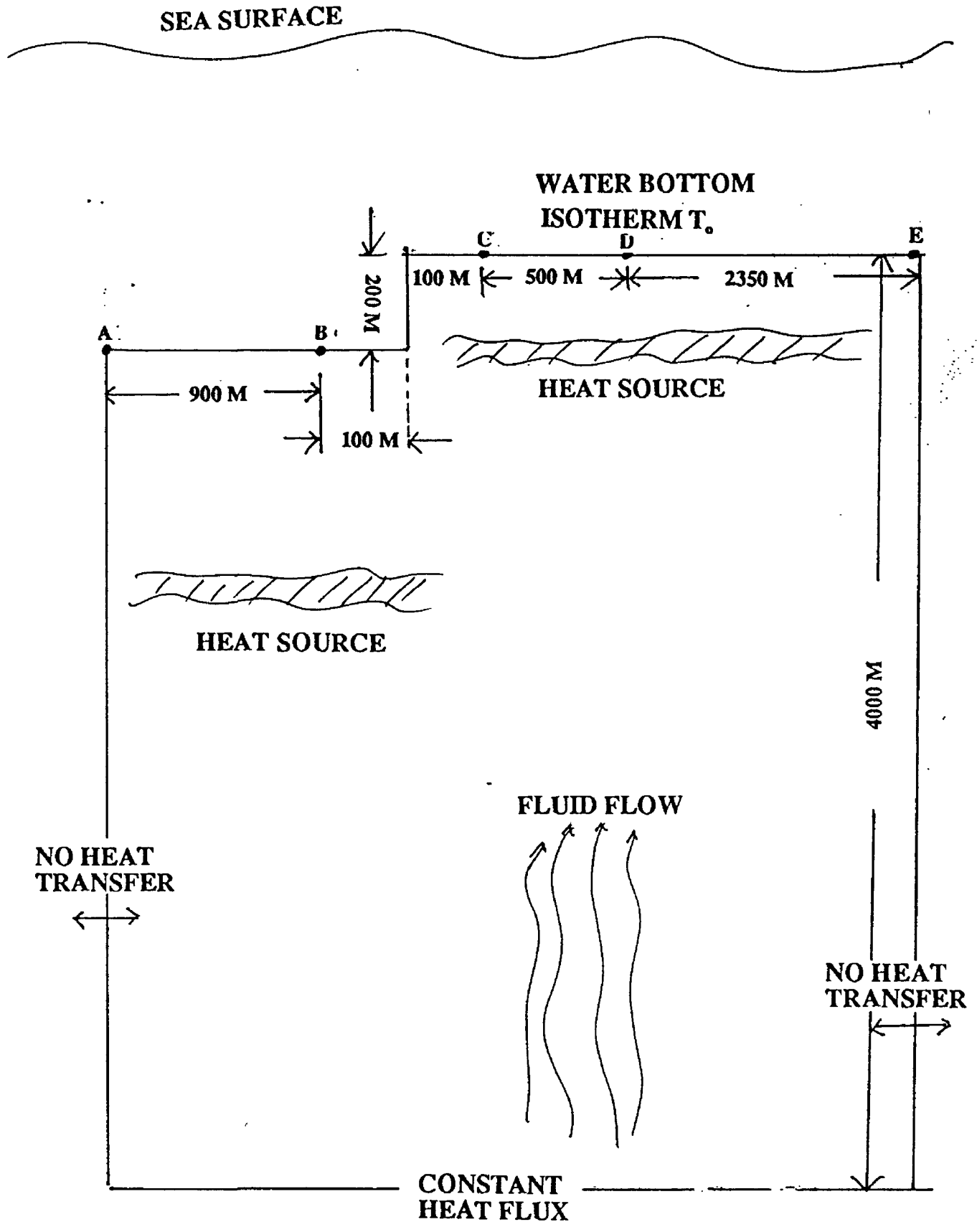


Figure 1. A schematic diagram (model) for a landslide with 200 m scar. A, B, C, and D are locations used in the analysis. Two internal heat sources, one at the near surface sediment and the other at the BSR level, and advective fluid flow are modeled in order to predict the BSR depths.

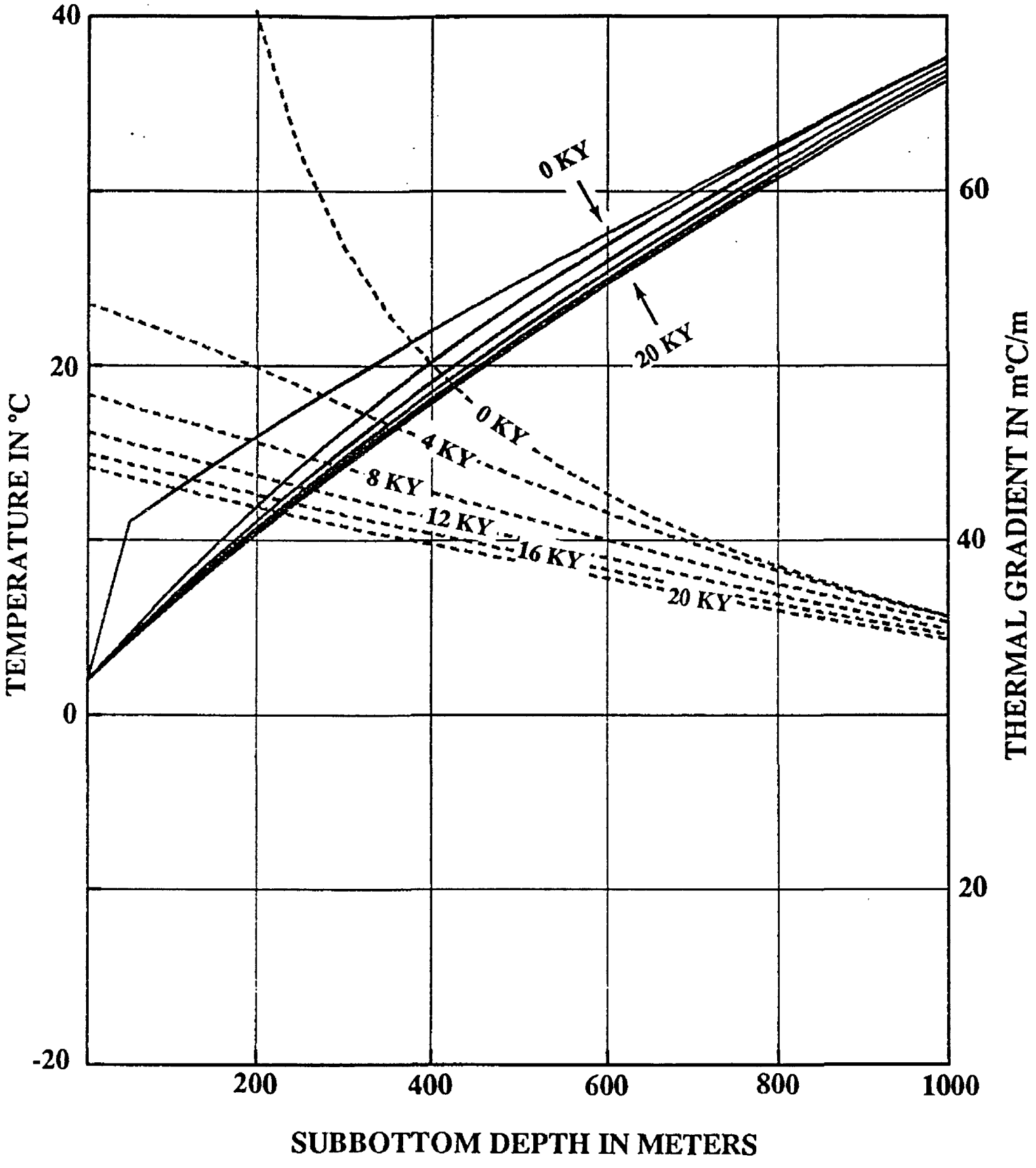


Figure 2. Temperatures (solid lines) and average thermal gradients (dashed lines) at location A (Figure 1) for the first 20,000 years at 4,000 year time intervals, without a heat source or advective flow, using the landslide model shown in Figure 1. The model parameters are $T_o = 2.0°C$ and $Q = 38\ mW/m^2$ (a constant heat flux boundary condition at the depth of 4,000 m). KY is 1,000 years.

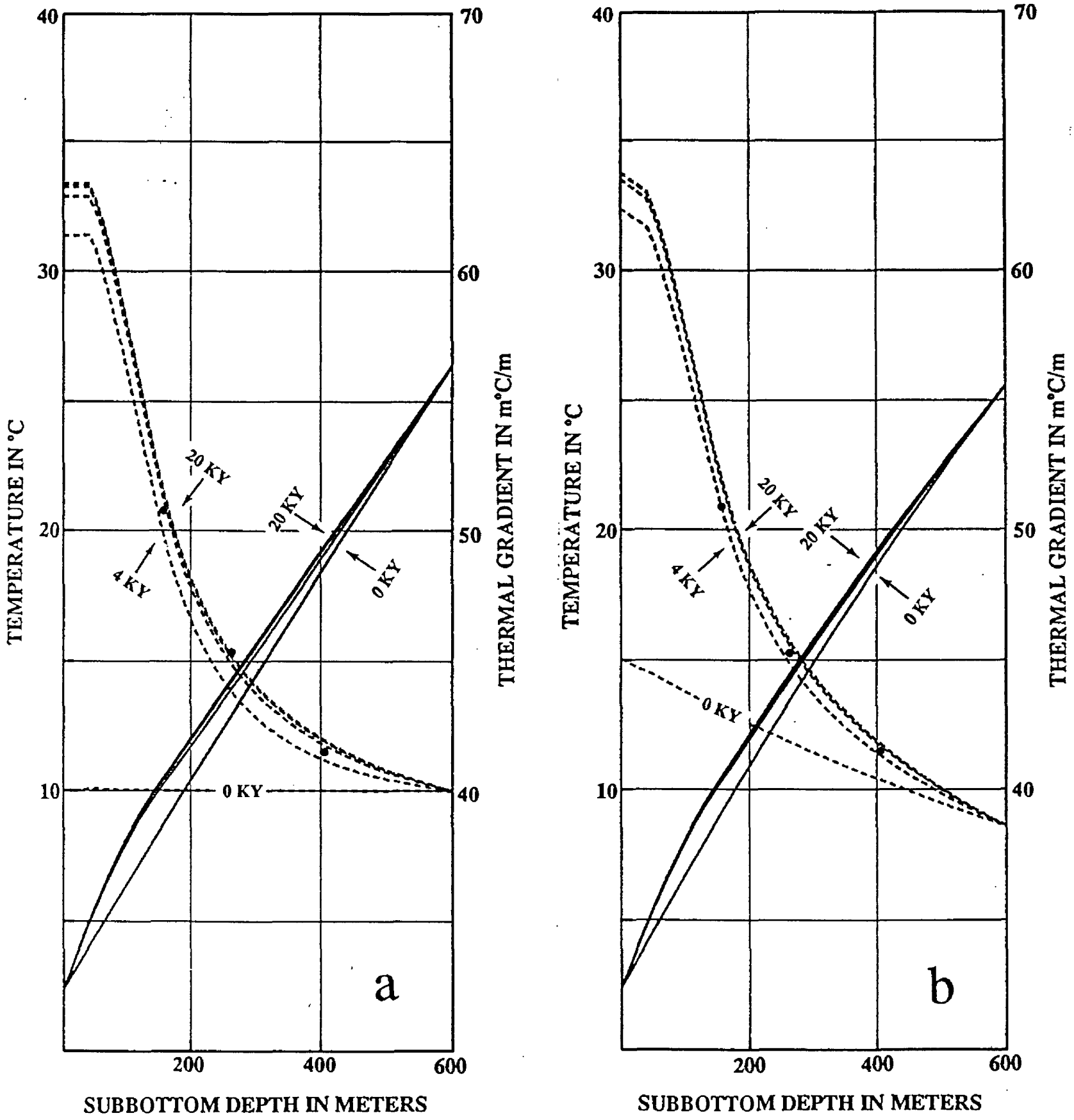


Figure 3. Temperatures (solid lines) and average thermal gradients (dashed lines) for the first 20,000 years at 4,000 year time intervals for an one-dimensional heat source uniformly located between 40 m and 140 m in depth with $T_o$ = 2.4°C and a constant temperature boundary condition at the depth of 600 m . The dots indicate the measured average thermal gradients at the DSDP 533. a) Constant conductivity (1.0 $Wm^{-1}K^{-1}$) with Q = 40 $mW/m^2$ at the depth of 600 m and H = 250 $\mu Wm^{-3}$ b) Depth-dependent conductivity with Q = 44 $mW/m^2$ and H = 200 $\mu Wm^{-3}$ at the depth of 600 m. KY is 1,000 years.

The constant temperature boundary condition at the lower boundary was used for both figures, and in the case of depth-dependent thermal conductivity, the constant temperature was computed by the one-dimensional steady-steady finite difference equation assuming that there is no heat source. The dots in Figure 3 are measured average thermal gradients at the DSDP hole 533 and will be discussed later. Notice the average thermal gradient is increased from an initial value of 40 m°C/m to 63 m°C/m in 20,000 years for the constant thermal conductivity medium and from 45 m°C/m to 63 m°C/m for the depth-dependent thermal conductivity. Because the thermal conductivity increases with depth, the initial thermal gradient before the source is emplaced decreases with depth.

## STEADY STATE SOLUTION

### A) Two-Dimensional Solution

A two-dimensional steady-state equation can be easily derived from Equation (4) by deleting the terms $T_{i,j}^{n+1}$ and the last term $T_{i,j}^{n}$ in Equation (4) and setting $\Delta t = 1$. The equation can be solved approximately by the Gauss-Seidel iterating method (Carnahan and others, 1969). In other words, the solution can be obtained by the repeated application of

$$T_{i,j} \leftarrow F(T_{i-1,j}, T_{i+1,j}, T_{i,j-1}, T_{i,j-1}, H_{i,j})$$

in the finite difference equation. Reasonable initial temperatures at the grid points are important in solving the steady-state equation.

The steady-state solution for the landslide model without a local heat source or an advective fluid flow is given in Figure 4. A constant heat flux at the depth of 4,000 m with $Q=38$ mW/m$^2$ was used. The average gradient at location A is about 41 m°C/m, while it is about 44 m°C/m at 20,000 years (Figure 2). The steady-state temperature at the depth of 600 m at point A as indicated in Figure 4 is about 2 degrees less than the temperature should be at 20,000 years after slide occurred as indicated in Figure 2. The high thermal gradient at location B and the low thermal gradient at location C is due to the lateral heat transfer between the cold region and the hot region across the edge of the slide area.

### B) One-Dimensional Solution

For the one-dimensional case, the finite difference equation can be written as:

$$\begin{aligned}\frac{(k_{j+1/2}+4k_j-k_{j-1})}{4\Delta z^2}T_{j+1} = {} & \frac{4k_j}{\Delta z^2}T_j + \frac{(-k_{j+1}+4k_j+k_{j-1})}{4\Delta z^2}T_{j-1} \\ & + \frac{\beta_j^o}{2\Delta z}(\phi_{j+1}F_{j+1}^z T_{j+1} - \phi_{j-1}F_{j-1}^z T_{j-1}) \\ & + \frac{\beta_j}{2\Delta z}\{(1-\phi_{j+1})S_{j+1}^z T_{j+1} - (1-\phi_{j-1})S_{j-1}^z T_{j-1}\} \\ & - H_j \end{aligned} \qquad (8)$$

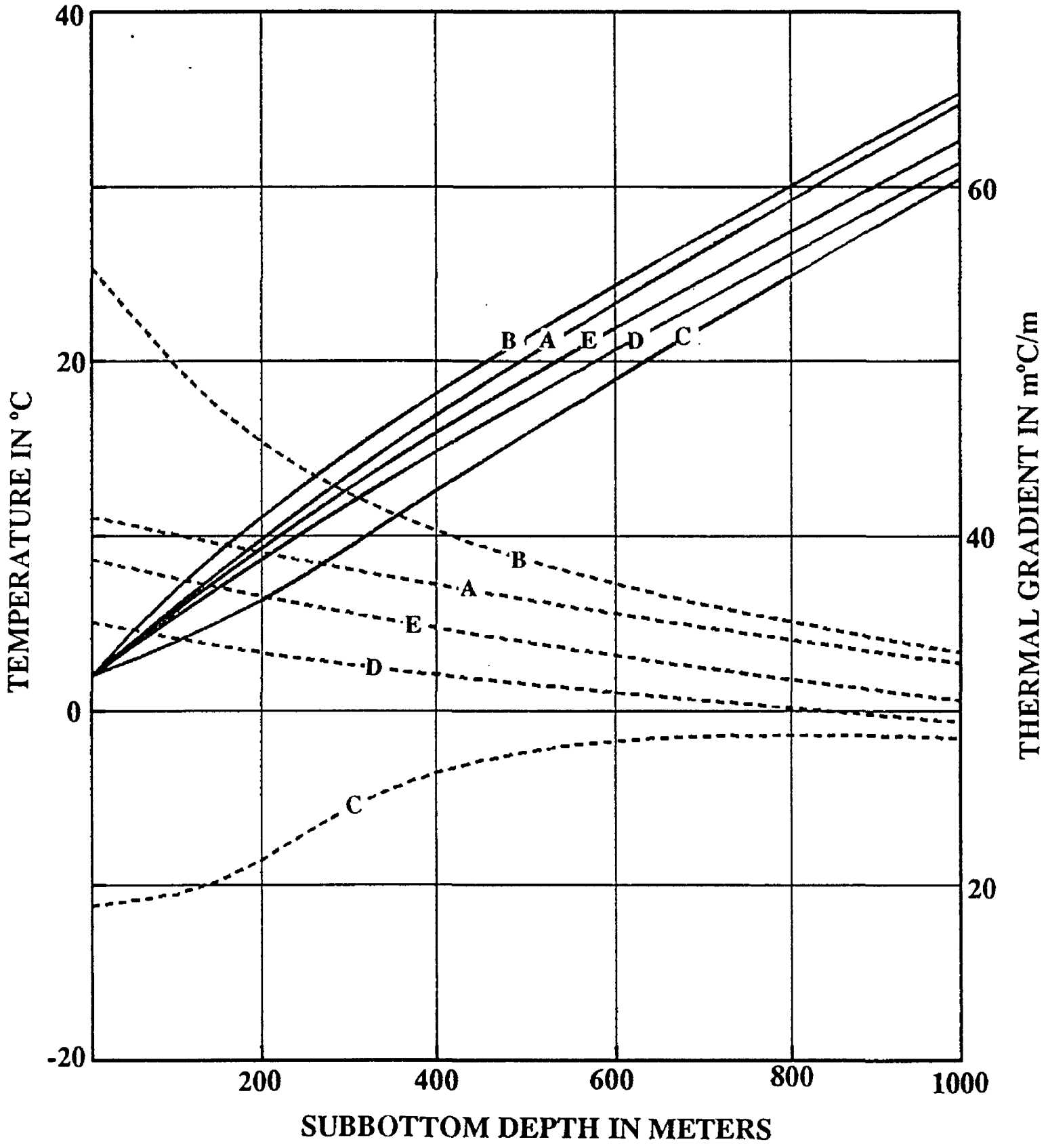


Figure 4. Steady-state temperatures (solid lines) and average thermal gradients (dashed lines) at 5 locations (Figure 1) without a local heat source or advective flow for the landslide model. The model parameters are $T_o$ = 2.0°C and Q = 38 mW/m$^2$ (a constant heat flux boundary condition at the depth of 4,000 m).

The solution of Equation (8) with boundary conditions of the constant temperatures at the top and bottom of the model can be written by the following matrix equation.

$$\begin{pmatrix} 1 & 0 & . & . & . & . \\ c_2 & b_2 & a_2 & . & . & . \\ 0 & c_3 & b_3 & a_3 & . & . \\ . & . & . & . & . & . \\ . & . & . & . & . & . \\ . & . & . & c_{J-1} & b_{J-1} & a_{J-1} \\ . & . & . & . & 0 & 1 \end{pmatrix} \begin{pmatrix} T_1 \\ T_2 \\ T_3 \\ . \\ . \\ T_{J-1} \\ T_J \end{pmatrix} = \begin{pmatrix} Boundary \\ -H_2 \\ -H_3 \\ . \\ . \\ -H_{J-1} \\ Boundary \end{pmatrix}, \quad (9)$$

where

$$a_j = \frac{k_{j+1} + 4k_j - k_{j-1}}{4\Delta z^2} - \frac{\beta_j^o \phi_{j+1} F_{j+1}^z}{2\Delta z} - \frac{\beta_j (1-\phi_{j+1}) S_{j+1}^z}{2\Delta z},$$

$$b_j = -8\frac{k_j}{\Delta z^2},$$

$$c_j = \frac{-k_{j+1} + 4k_j + k_{j-1}}{4\Delta z^2} + \frac{\beta_j^o \phi_{j-1} F_{j-1}^z}{2\Delta z} + \frac{\beta_j (1-\phi_{j-1}) S_{j-1}^z}{2\Delta z}.$$

"Boundary" in Equation (9) denotes the boundary temperature. If the constant flux instead of the constant temperature is used at the bottom of the model, the bottom row of Equation (9) should be changed (0 changed into -1 and the value for the boundary is $Q_B/k_J$). In contrast to the two-dimensional steady-state solution, this tri-diagonal matrix equation can be solved very effectively (Wachspress, 1960).

An example of calculated steady-state temperatures and average thermal gradients is shown in Figure 5. Parameters for Figure 5 are $T_o = 2.4°C$, $H = 200\ \mu W m^{-3}$ between 40 m and 140 m in depth, with a constant heat flux boundary condition of $Q = 40\ mW/m^2$ at the depth of 4000 m was applied. The curve for steady-steady temperature for the depth-dependent thermal conductivity (Figure 5) is almost identical to the temperature curve shown in Figure 3b. Considering that parameters for two figures are quite different, particularly for the boundary condition at the lower boundary, it is clear that the inverse problem in the real data analysis may not provide a unique solution. In other words, many thermal models fit the observations.

One-dimensional steady-state solutions are very important in implementing the initial conditions for either steady or non-steady state solutions. For example, the initial temperature for a model shown in Figure 4 was derived by solving the corresponding one-dimensional difference equation.

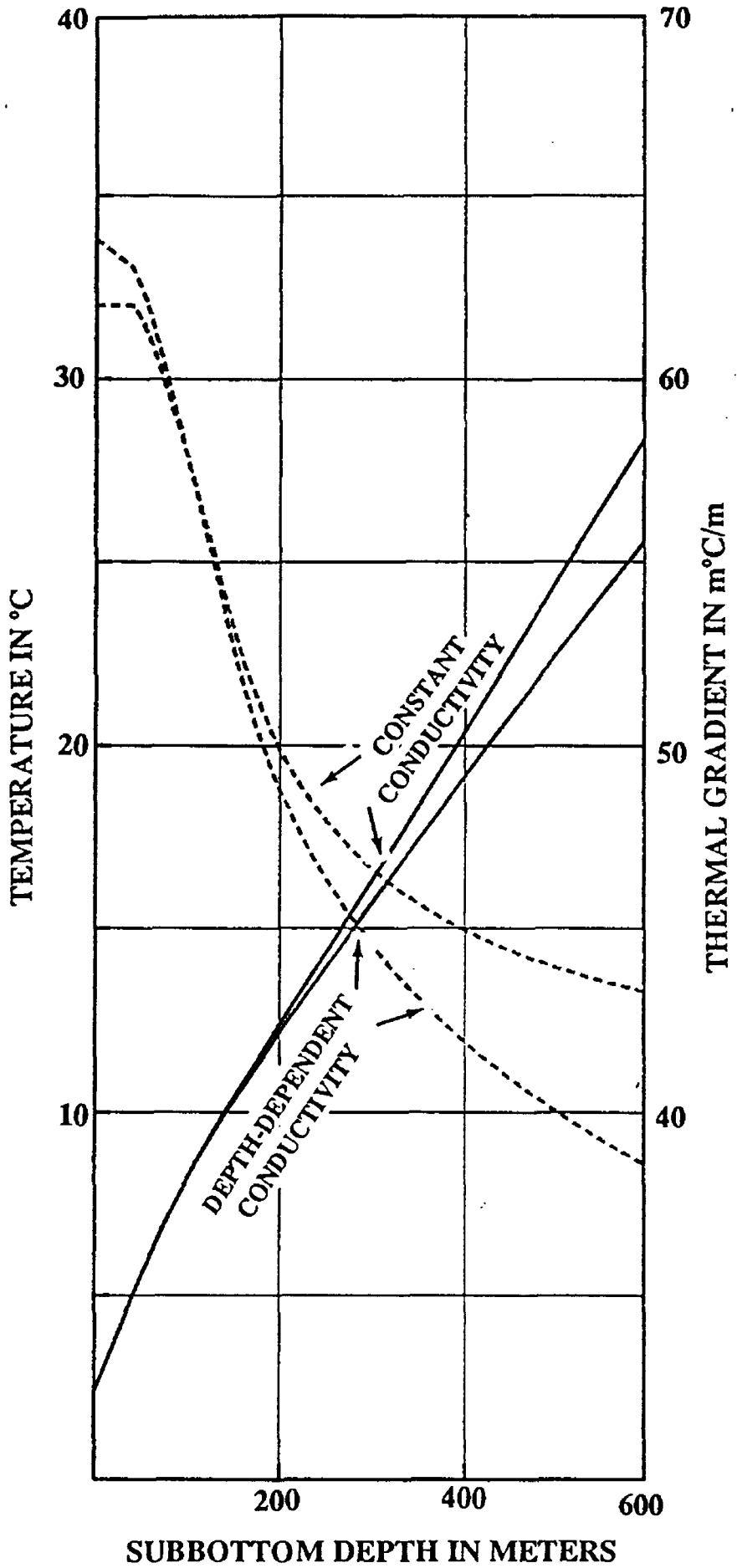


Figure 5. Steady-state temperatures (solid lines) and average thermal gradients (dashed lines) for one-dimensional heat source model, assuming either constant or depth-dependent thermal conductivity. Uniform heat source is located between 40 m and 140 m in depth with a magnitude of H = 200 $\mu W m^{-3}$. Other model parameters are $T_o$ = 2.4°C and Q = 40 mW/m$^2$ (a constant heat flux boundary condition at the depth of 4,000 m).

## SIMPLE ANALYTIC SOLUTIONS

The analytic solution of one-dimensional heat flow equation without a heat source or an advective term under the assumption of homogeneous medium can be easily derived. Let the initial condition be

$$T(z,0) = T_o^* + \frac{T_l - T_0^*}{l} z,$$

and the constant temperature boundary conditions be

$$T = T_o \quad \text{at} \quad z = 0 \quad \text{and} \quad T = T_l \quad \text{at} \quad z = l.$$

Then the solution can be written as follows using the solution form of Hildebrand (1963) and the Fourier series.

$$T = T_o + \frac{(T_l - T_o)}{l} z + \sum_{n=1}^{\infty} \frac{2\Delta T}{n\pi} \sin\frac{n\pi z}{l} \exp\left(-\frac{n^2\pi^2 k t}{l^2 \beta}\right) \tag{10}$$

$\Delta T$ is the difference between initial temperature and the boundary condition at z = 0:
$\Delta T = T_0^* - T_0$.

If the constant heat flux instead of the constant temperature at z = $l$ is used , the solution can be written as:

$$T = T_o + \int_0^z \frac{Q_l}{k} dz + \sum_{n=0}^{\infty} \frac{2\Delta T}{(n+1/2)\pi} \sin\frac{(n+1/2)\pi z}{l} \exp\left(-\frac{(n+1/2)^2\pi^2 k t}{l^2 \beta}\right), \tag{11}$$

and $Q_l$, the heat flux at z = $l$, is kept constant.

These solutions indicate that the time required for the steady-state condition is dependent on the boundary conditions and the constant flux boundary condition requires more time to reach the steady state condition. The term inside the summation represents the time-dependent (or transient) temperature and Table 1 shows the contribution of these terms with respect to time.

| Elapsed Time In Years | Time-Variant Temperature (°C) Using Constant Temperature Boundary Condition | Time-Variant Temperature (°C) Using Constant Heat Flux Boundary Condition |
|---|---|---|
| 50,000 | 2.80 | 4.83 |
| 100,000 | 1.60 | 3.63 |
| 250,000 | 0.42 | 2.32 |
| 500,000 | 0.048 | 1.34 |
| 1,000,000 | 0.0006 | 0.45 |

Table 1. The temperature variation with respect to time for two different boundary conditions at the lower boundary. The lower boundary condition is emposed at 3800 m, the temperature difference at z=0 is 8 °C, and the transient temperature measured at z = 1000 m.

The model parameters are $l$ = 3800 m, $\Delta T$ = 8°C, z = 1000 m, and $Q_l$ = 38 mW/m$^2$. As indicated in Table 1, by applying the constant temperature boundary condition at the lower boundary the temperature reaches the steady-state condition faster than by applying the constant flux boundary condition. At 250,000 years, the time-dependent temperature term is 0.42 °C for the constant temperature boundary condition and 2.32 °C for the constant heat flux boundary condition.

Figure 6 shows the numerical solutions for the previous model for the first 1 million years at 200,000 year time increments and the result of this figure confirms the analysis of the analytic solution. The dots in Figure 6b show the analytic solutions at 200,000 years and show an excellent agreement between the finite difference solutions and the analytic solutions. Because of the imposed boundary condition (no lateral heat transfer) at location A, the two-dimensional solution at location A is identical to the one-dimensional solution. The average temperature difference between the numerical and analytic solutions at 5 locations (200m, 400m, 600m, 800m, and 1000m in Figure 6b) is 0.05 °C at 200,000 years. Therefore, the numerical solutions in this paper do not have a gross error in the temperature of the sediments.

## DISCUSSION

### A) THERMAL CONDUCTIVITY

One of the effects of high thermal conductivity in a heat flow equation is to reduce the time required to reach the steady-state condition. Solutions shown in Equations (10) and (11) indicate that system should take less time to reach the steady-state condition if the higher thermal conductivity is assumed. Figure 3 also indicates the same implication.

The steady-state solution shown in Figure 5 indicates that when the heat flux is constant at great depth, the average thermal gradient is lower for the depth-dependent thermal conductivity model (increasing conductivity with depth) than that for the constant thermal conductivity model. At 600 m in Figure 5, the average thermal gradient is about 39 m°C/m for the depth-dependent thermal conductivity case (its heat flow is about 44.6 mW/m$^2$ using the average thermal conductivity of 1.146 $Wm^{-1}K^{-1}$) and about 43 m°C/m for the constant thermal conductivity case (its heat flow is 43 mW/m$^2$ using the thermal conductivity of 1.0 $Wm^{-1}K^{-1}$). The lower average thermal gradient for the depth-dependent thermal conductivity has a significant implication on the BSR depth. Let's assume that the temperature at the BSR phase boundary is 25 °C. Figure 5 indicates that the BSR depth for constant thermal conductivity is about 510 m and 575 m for depth-dependent thermal conductivity. So the reduction in porosity or increase in thermal conductivity provides a deeper BSR depth.

The effect of depth-dependence of thermal conductivity in hydrate-bearing sediments may be reduced compared to non-hydrate-bearing sediments, because the hydrate might cement the grains and prevent compaction and the thermal conductivity of hydrate is a little lower than for pure water. However, the hydrate cementation in marine sediments is low (Lee and others, 1993), so the compaction effect may be dominant over the effect of hydrate cementation for the computation of temperature that would control the hydrate phase boundary.

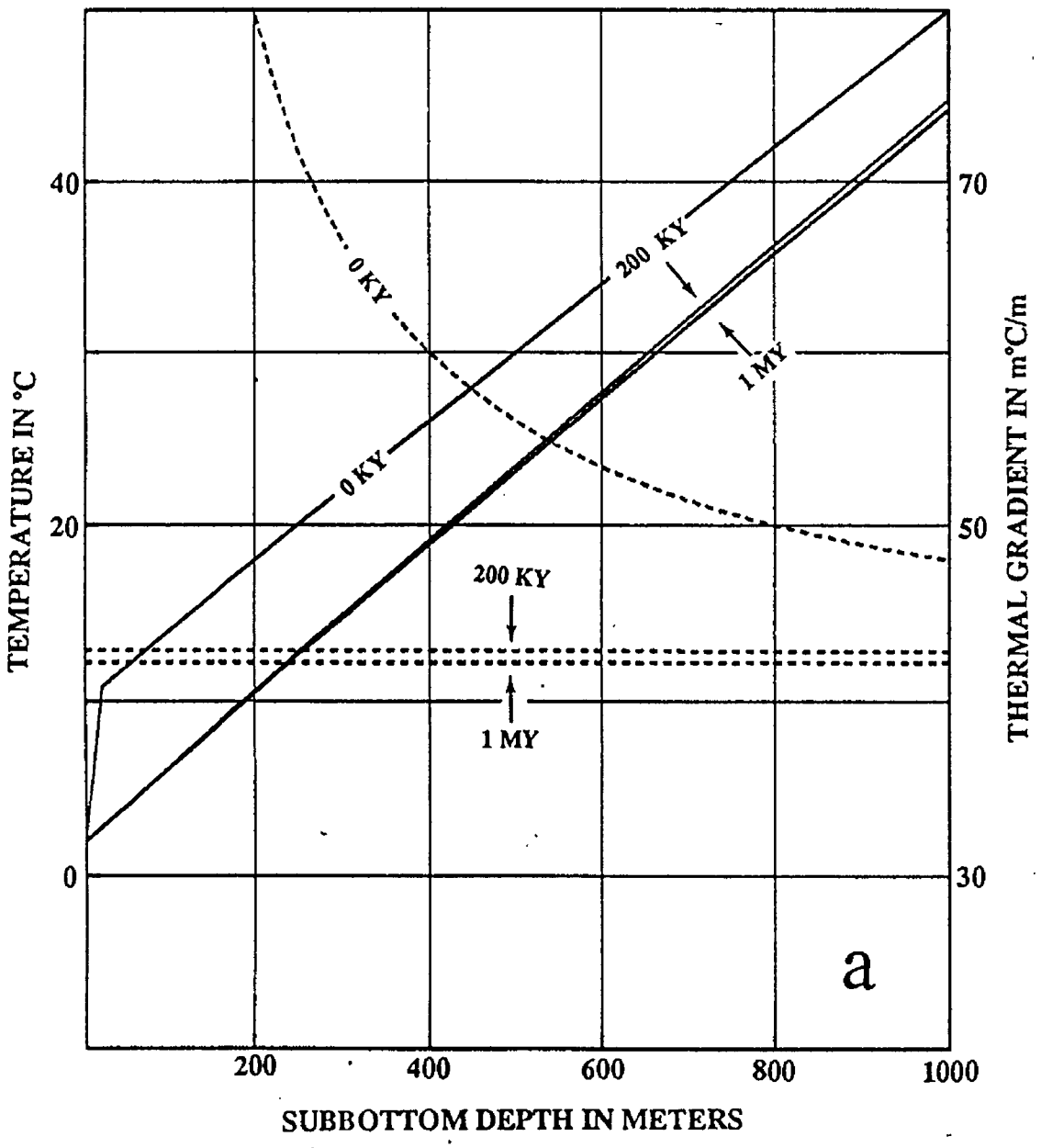


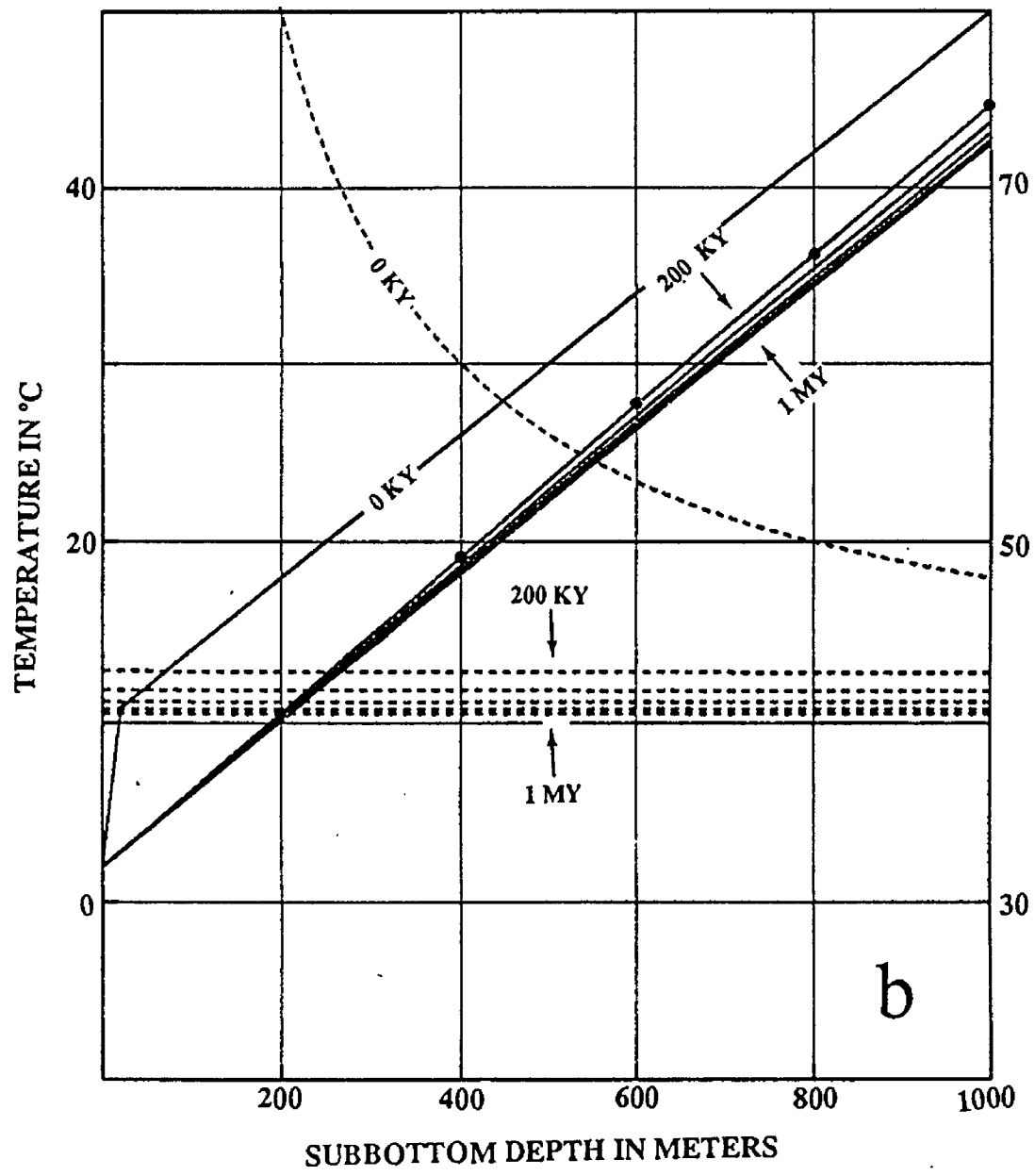


Figure 6. Temperatures (solid lines) and average thermal gradients (dashed lines) at the location A (Figure 1) for the landslide model. The model was run for the first 1,000,000 years at 200,000 year time intervals without a heat source or advective flow with $T_o = 2.0°C$ and $Q = 38$ mW/m$^2$ at the depth of 4,000 m. KY is 1,000 years and MY is 1,000,000 years. a) Constant temperature boundary condition at the depth of 4,000 m. b) Constant heat flux boundary condition at the depth of 4,000m. The dots on Figure 6b are analytic solutions.

## B) DSDP 533

The average thermal gradients computed by the measured temperatures at DSDP 533 (Sheridan and Gradstein and others, 1970) are indicated as dots in Figure 3. The average thermal gradients are 51 m°C/m, 45 m°C/m, and 42 m°C/m at the well depths of 155.5 m, 255.8m, 400m respectively. The observed BSR depth from the seismic profile at the DSDP 533 is about 515 m when using the average interval velocity of 1.723 km/s (Lee and others, 1992). If the average thermal gradient computed from the temperature at 155.5 m is used for the BSR depth computation, the predicted BSR depth is 436 m (The parameters for the BSR depth computation are $T_o$ = 2.4°C, water depth = 3200 m, depth-dependent thermal conductivity, lithostatic pressure (sediments density is assumed to be 1.875 times of the sea water), and phase diagram for 100 % methane in 3.5 % NaCl water (Macleod, 1982)). On the other hand, when the measurement at the well depth of 400 m is used, the predicted BSR depth is 551 m, which is much closer to the observed BSR depth .

Figure 3 indicates that the depth-dependent thermal gradients at the well can be explained by introducing a uniform heat source of 200 $\mu Wm^{-3}$ located between 40 m and 140 m in depth when using the depth-dependent conductivity or by introducing a uniform heat source of 250 $\mu Wm^{-3}$ located between 40 m and 140 m in depth when using the constant conductivity medium. Possible heat sources are heat generated from the conversion of organic matter into biogenic gas in the anaerobic zone and heat generated from transforming gas into hydrate. The thermal gradient computed at 4,000 years after the emplacement of the source is similar to that computed at 20,000 years. So this internal source model does not provide accurate information about the time of source emplacement, but this model emphasizes that the depth-dependent thermal gradient can be reasonably well explained by introducing a heat source.

Figure 7 shows the temperature and average thermal gradient computed using parameters which are $T_o$ = 2.4°C, $l$ = 4000 m, Q = 42 mW/m$^2$ at $l$ = 4000 m, H = 200 $\mu Wm^{-3}$ located between 40 m and 140 m in depth, and the constant heat flux boundary condition. The lower boundary condition imposed on two models shown in Figure 3 may not be realistic ( the depth to the constant temperature or constant heat flux is too shallow), but the temperature distribution is similar to those shown in Figure 3. The results of Figures 3 and 7 demonstrate that as long as there are uncertainties in the heat flow measurements, there may not be a unique model to fit the observation. Notice the differences in the boundary conditions and heat flow at the lower boundary in Figures 3 and 7.

## C) SLIDE AREA

Figure 8 shows a seismic profile crossing a recent landslide area and shows a variable BSR depths along the profile. The observed BSR depths and inferred heat flows at selected locations on the seismic profile 3 are shown in Table 2. The average inferred heat flow, estimated from the BSR depths, within the slide scar area is about 55 mW/m$^2$ and about 39 mW/m$^2$ at the outside area. Table 2 indicates that the subbottom depth to the BSR in the slide scar area is about 200 m shallower than BSR depths outside area. Let's assume that the water depth at the adjacent area is 4,000 m and 200 m of sediments have slid away at the slide area. Then the temperature at the methane hydrate phase boundary in 3.5% NaCl water when using parameters of $T_o$ = 2°C, the depth-dependent thermal conductivity, and lithostatic pressure is 24.74 °C at the slide area and 24.43 °C at the adjacent area.

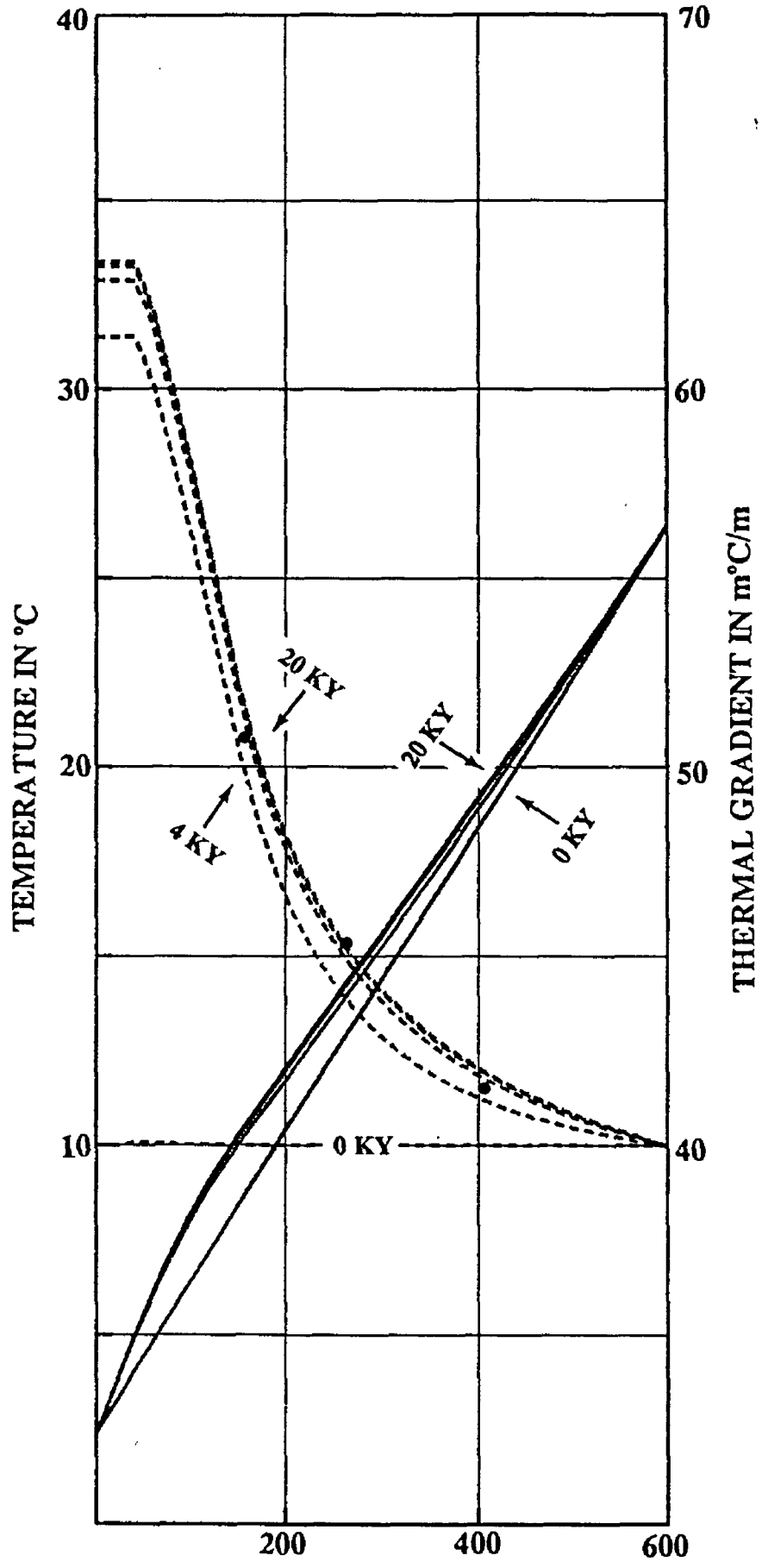


Figure 7. Temperatures (solid lines) and average thermal gradients (dashed lines) for an one-dimensional heat source uniformly distributed between 40 m and 140 m with a magnitude of 200 $\mu W m^{-3}$. Time is for the first 20,000 years at 4,000 year time intervals. Other model parameters are $T_o = 2.4°C$ and $Q = 42$ mW/m$^2$ (a constant heat flux boundary condition at the depth of 4,000 m). The dots indicate the measured average thermal gradients at the DSDP 533. KY is 1,000 years.

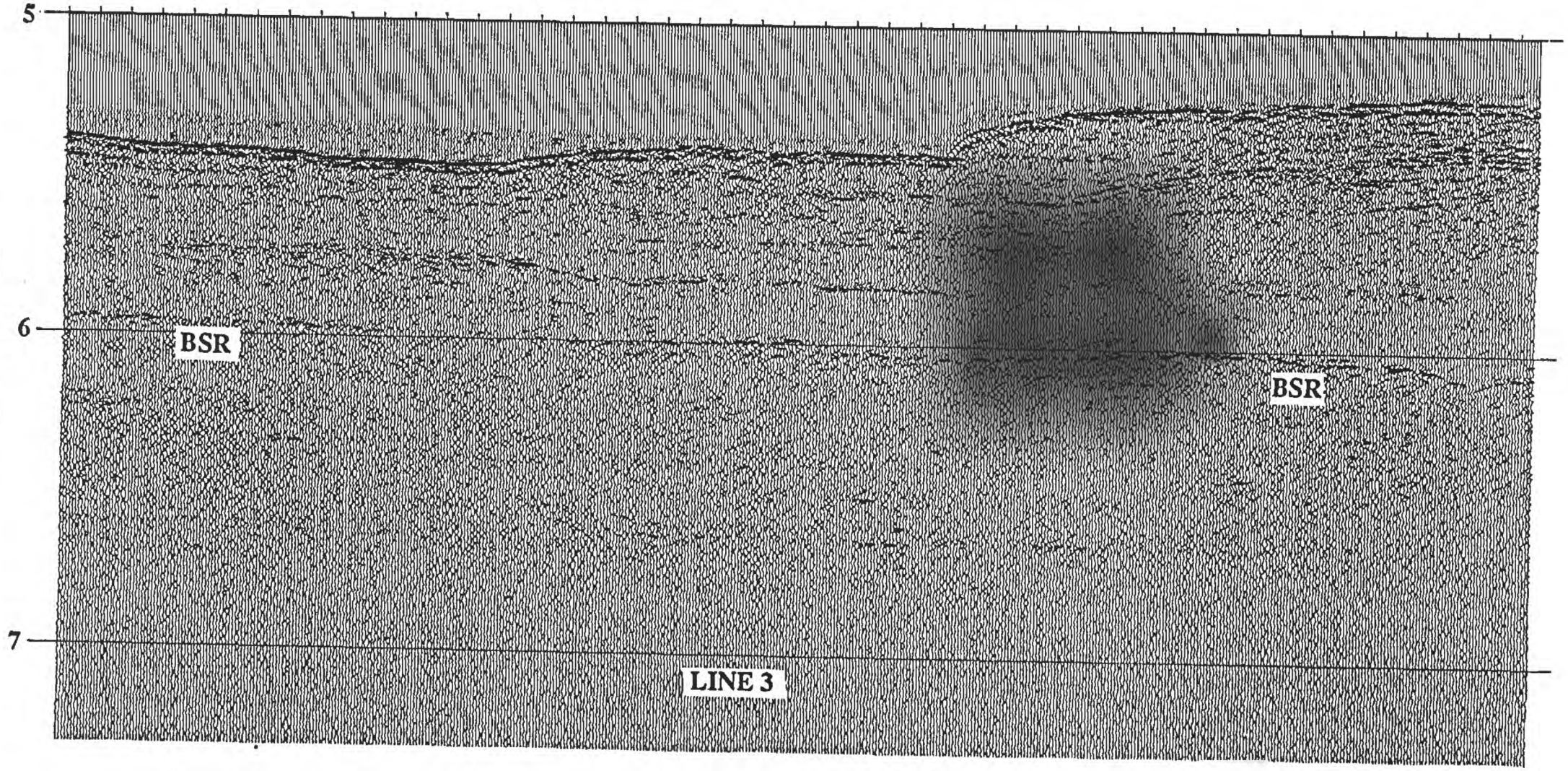


Figure 8. A seismic profile crossing a recent landslide in the Carolina Rise area.

| Depth (m) | Observed BSR Depth (m) | Inferred Heat Flow ($mW/m^2$) |
|---|---|---|
| 3930 | 685 | 37.9 |
| 3935 | 655 | 37.3 |
| 3947 | 651 | 39.5 |
| 3946 | 647 | 39.7 |
| 4071 | 544 | 46.2 |
| 4060 | 540 | 46.5 |
| 4110 | 454 | 54.0 |
| 4108 | 445 | 54.9 |
| 4086 | 463 | 53.0 |

Table 2. Observed BSR depths and inferred heat flows along seismic profile 3. The parameters for the computation of heat flows inferred from the BSR depths are $T_o = 2°C$, lithostatic pressure, and a hydrate phase diagram for pure methane in 3.5% NaCl water. In order to derive the porosity variations with depth, and the resulting depth-dependent thermal conductivities, surface conductivities of 1 $Wm^{-1}K^{-1}$ were used.

Figure 9a shows the temperatures and average thermal gradients at 5 locations shown in Figure 1 at 2,000 years after the slide without any internal heat source or advective flow and Figure 9b shows the temperatures and gradients at 20,000 years with similar conditions. Using the temperature and pressure appropriate to the gas hydrate phase boundary, I have shown the expected depths of BSR inside the slide scar (triangles) and outside it (dots) for times of 2000 years after the slide (Figure 9a) and 20,000 years after the slide (Figure 9b). It is shown that the difference of subbottom depths to the BSR between the slide area (curves labelled A) and the adjacent area (curves labelled E) is about 200 m after 2,000 years and about 80 m in 20,000 years. As far as the subbottom depth to the BSR is concerned, the younger slide model fits the observations better than the older slide model. Figure 9a predicts a heat flow difference of about 20 $mW/m^2$ between the slide and adjacent area (between locations A and E), whereas Figure 9b predicts a difference of about 5 $mW/m^2$.

Numerical solutions that include internal heat sources are shown in Figures 10 and 11 using the model shown in Figure 1. The steady-state solution for this model is shown in Figure 10 and temperatures at 2000 years and 10,000 years after the slide are shown in Figures 11a and 11b respectively. Figure 10, the steady-state solution, predicts that the subbottom depth to the BSR at location A is 430 m and the surface heat flow is 57 $mW/m^2$. At location E, the subbottom depth to the BSR is 670 m and the surface heat flow is 46 $mW/m^2$. The results of this model fit the observed BSR depths reasonably well at both locations.

Inferred heat flow value computed from the BSR depth should be very similar to the heat flow value measured at the surface, if there is no internal heat sources and/or advective fluid flows between the surface and the BSR depths.

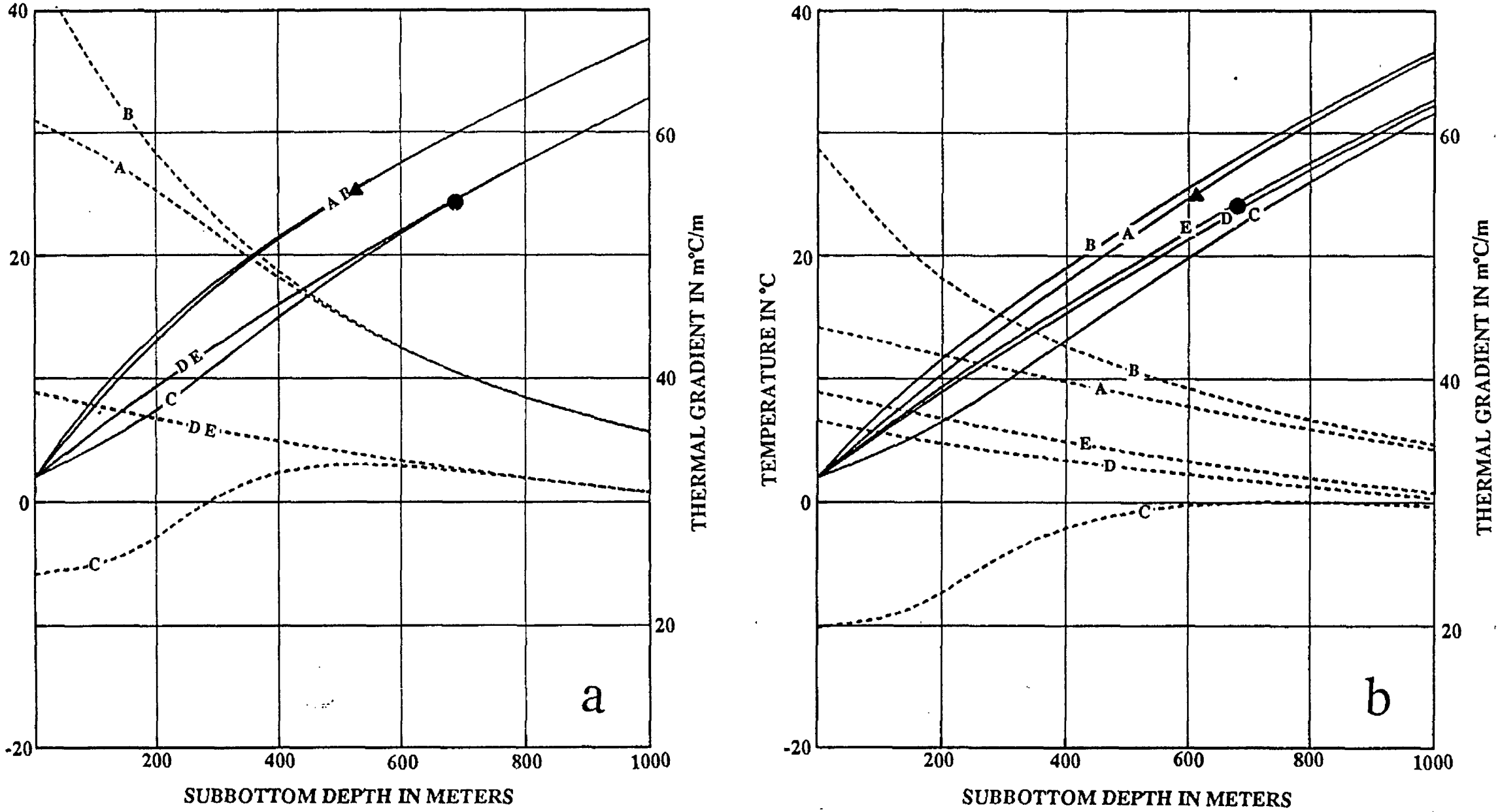


Figure 9. Temperatures (solid lines) and average thermal gradients (dashed lines) at 5 locations (Figure 1) without a heat source and advective fluid flow for the landslide model. Triangles denote the calculated BSR depth at location A and dots at location E. Other model parameters are $T_o = 2.0°C$ and $Q = 38$ mW/m$^2$ (a constant heat flux boundary condition at the depth of 4,000 m). a) At 2,000 years after landslide. b) At 20,000 years after landslide.

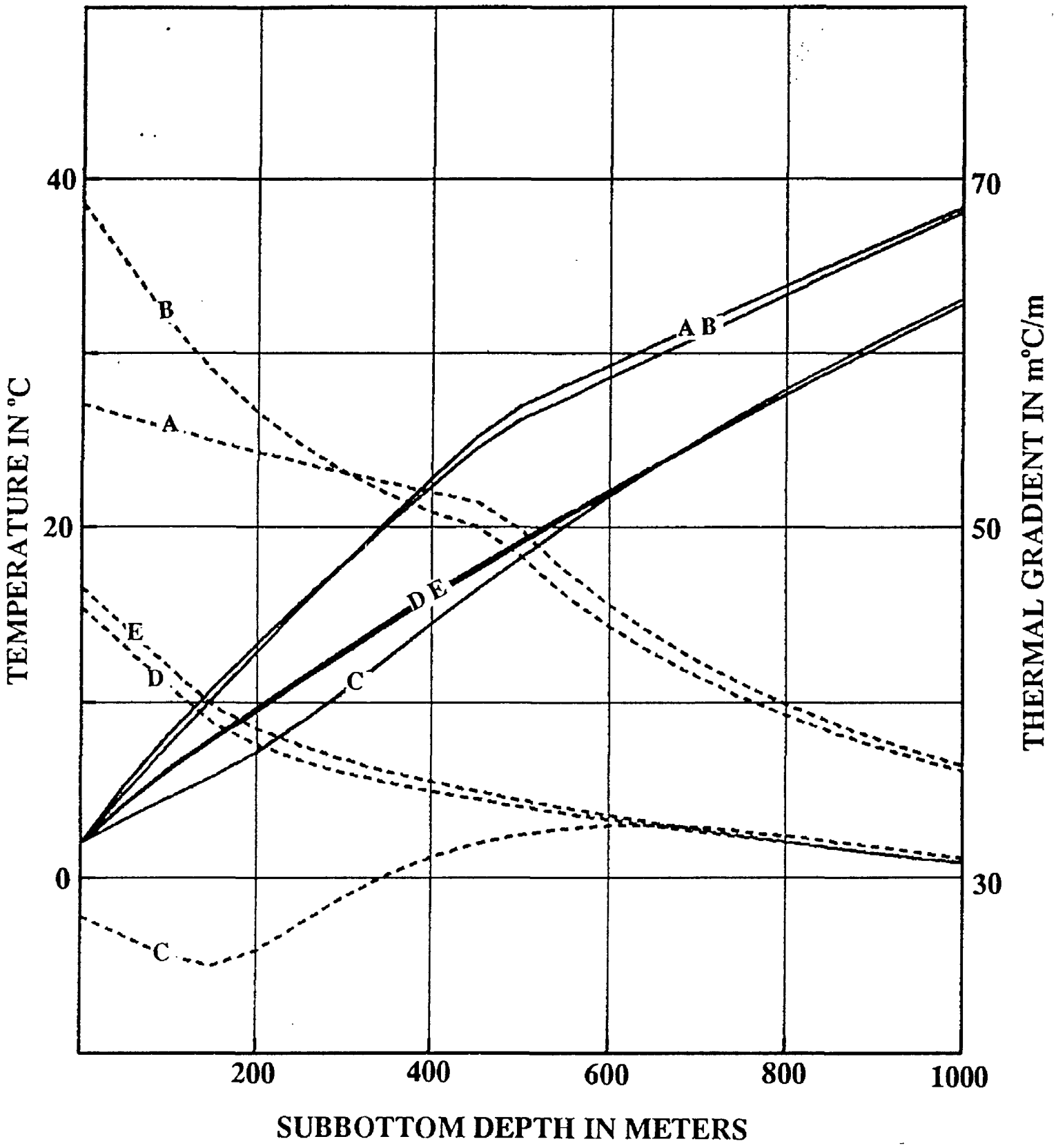


Figure 10. Steady-state temperatures (solid lines) and average thermal gradients (dashed lines) at 5 locations (Figure 1) with two local heat sources for the landslide model. Other model parameters are $T_o$ = 2.0°C and Q = 38 mW/m$^2$ (a constant heat flux boundary condition at the depth of 4,000 m). The local heat source in the slide scar area is H = 300 $\mu W m^{-3}$ located between 450 m and 550 m in depth and the other source in the adjacent area is 67 $\mu W m^{-3}$located between 50 m and 150 m in depth.

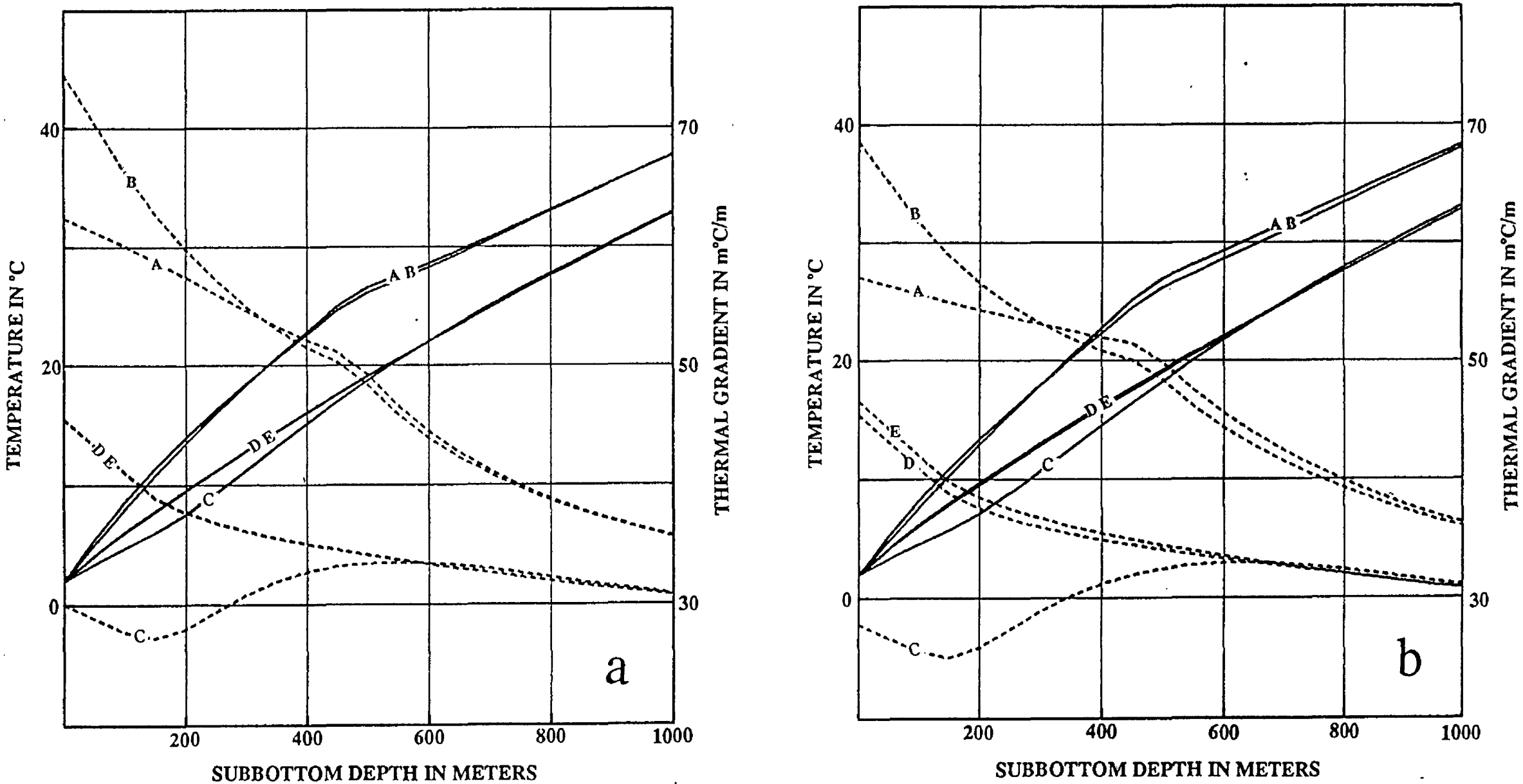


Figure 11. Temperatures (solid lines) and average thermal gradients (dashed lines) at 5 locations (Figure 1) with two local heat sources for the landslide model. Other model parameters are $T_o$ = 2.0°C and Q = 38 mW/m$^2$ (a constant heat flux boundary condition at the depth of 4,000 m). The local heat source in the slide scar area is H = 300 $\mu Wm^{-3}$ located between 450 m and 550 m in depth and the other source in the adjacent area is 67 $\mu Wm^{-3}$located between 50 m and 150 m in depth. a) At 2,000 years after slide. b) At 10,000 years after slide.

The average heat flow value of 37 mW/m$^2$ at the adjacent undisturbed area, inferred from the observed BSR depth using seismic profile (Table 2), is almost identical to the steady state heat flow value I used for the model before the slide, but is 9 mW/m$^2$ less than the heat flow value predicted at the surface from the model. Because the predicted and observed BSR depths are similar to each other, I interpret that the difference of 9 mW/m$^2$ of heat flow value at location E is a thermal perturbation caused by a shallow internal heat source. Therefore a surface heat probe could overestimate the regional conductive heat flow value as much as 20 % in this case (about 46 mW/m$^2$ versus 37 mW/m$^2$). However, within the slide area, such as at location A, the heat flow value at the surface (57 mW/m$^2$) predicted from the model is similar to the average heat flow value inferred from the observed BSR depths. Because an internal heat source is located below the BSR level in this case, this internal source affects similarly both the surface heat measurement and the BSR depth.

Comparing the solutions of the model shown in Figures 11a and 11b with the steady-state solution in Figure 10, it is concluded that estimating the age of the slide based on the BSR depths and surface heat flow measurement may not be possible. Note that the temperature difference between the steady-state solution and the solution at 10,000 years is negligible.

The steady-state solution shown in Figure 4 predicts that when thermal equilibrium is reached after all internal heat sources are consumed and/or no more hydration occurs at the BSR level, the final subbottom depth to the BSR is about 620 m at location A and 680 m at location E. Therefore the BSRs observed in the seismic profile shown in Figure 8 represents a transient phenomena and as time progresses the BSR depths at the slide area will become deeper.

A physical mechanism for an internal heat source responsible for the high heat flow value or shallow BSR depths at the slide area can be explained by the following three-stage development of the BSR.

Stage 1 : Initial removing of mass at the slide area reduces the pressure at the previous BSR level. Since the thermal equilibrium cannot be achieved instantly, the initial reaction to the slide is to raise the BSR depth slightly. Let's assume that the conductive heat flow in this region before the slide is similar to the one observed adjacent to the slide area; namely 38 mW/m$^2$. Assume that the bottom water temperature is 2 °C and about 200 m of sediments was removed instantly. Just after the slide occurred, the pressure reduction, which would be instantaneous, would cause the base of hydrate stability to rise by 60 m; the temperature initially would be the same, and thus would have no effect. Therefore the subbottom depth of the BSR immediately after the slide would be reduced by the rise of the base of gas hydrate stability (60 m) and also reduced by the removal of sediment of the slide (200 m), so that the BSR after the slide would be 260 m shallower (subbottom) than before. Because of the shallowing of the base of gas hydrate stability in response to the reduced pressure, the hydrated sediments would be decomposed into free gas below the new phase boundary and would absorb heat.

Stage 2: As time goes on, thermal equilibrium would be established and the temperatures in the upper several, hundred meters would approach the regional temperature gradient values. During this time, the base of gas hydrate stability would become deeper in response to the decreasing sediment temperature. As the level of the phase boundary becomes deeper, the available free gas forms hydrate and the hydrate formation releases heat at the current BSR level.

Because the heat generation is at the BSR level, the observed heat flow at the sediment surface matches the heat flow inferred from the measured BSR depths. I interpret that the second stage is currently going on at the place where the seismic profile 3 (Fig. 8) is located.

Stage 3: When thermal equilibrium is established and no more hydrate is forming at the BSR level, the BSR depths will become close to the regional BSR depths. In this area, the BSR depths at the slide area will become about 620 m instead of the current depth of 450 m.

## D) HEAT SOURCE AND ADVECTIVE FLOW

The anomalously high heat flow measured at the surface compared to inferred heat flow from the BSR depths has been attributed to the advective fluid flow in the sediments (Davis and Hyndman, 1990). Figure 12a shows the temperature distribution at 2,000 years after the slide and Figure 12b shows the steady-state temperature with the advective vertical fluid flow. The amount of fluid flow is given by $-2.0e^{-10}\phi\ m/s$. Using the same temperature at the gas hydrate phase boundary for Figure 9, it is shown that the subbottom depths to the BSR at locations A and E are about 490 m and 670 m respectively and the difference of surface heat flow values between locations A and E is more than 20 $mW/m^2$. The younger slide model (Figure 12a) predicts a difference of about 200 m of BSR depths between the slide area and the adjacent area, and predicts that the difference of surface heat flow between locations A and E is much higher than those from the results shown in Figures 9 and 11. As also shown in Figure 9a, the younger slide model (2,000 years old) predicts a difference of about 200 m in the BSR depths, because the modeled scar is 200 m and there has not been enough time to reach the thermal equilibrium.

The steady-state solution of this model is similar to the steady-state solution without advective fluid flow shown in Figure 4. The steady-state solution indicates that the subbottom depths to the BSRs do not agree with the observations as opposed to the excellent agreement for a model assuming internal heat sources shown in Figure 10. Even though the model results using the internal heat source are better than those using the advective fluid flow, in order to test models accurately, near surface heat flow measurements are required.

The predicted steady-state surface heat flow value is 51 $mW/m^2$ at location A (Figure 12b) and the inferred heat flow value from the BSR depth is 43 $mW/m^2$. The advective fluid model also predicts an anomalous high heat flow at the surface compared to the heat flows inferred from the BSR depths, as demonstrated by Davis and Hyndman (1990). But the fluid flow model has a disadvantage compared to the internal source model regardless of the goodness of fit to the observation. It is well known that the low permeability of the hydrate-cemented sediments at the base of the hydrate stable layer causes reduction in permeability and trapping of free gas at the hydrate phase boundary and is the cause of the BSR (Dillon and Paull, 1983; Shipley and others, 1979). If this is the case, it is logical to assume that the fluid flow which affects the surface heat flow is confined only in the upper sediments above the BSR. This constraint introduces additional complication in the modeling and requires larger rates of fluid flow.

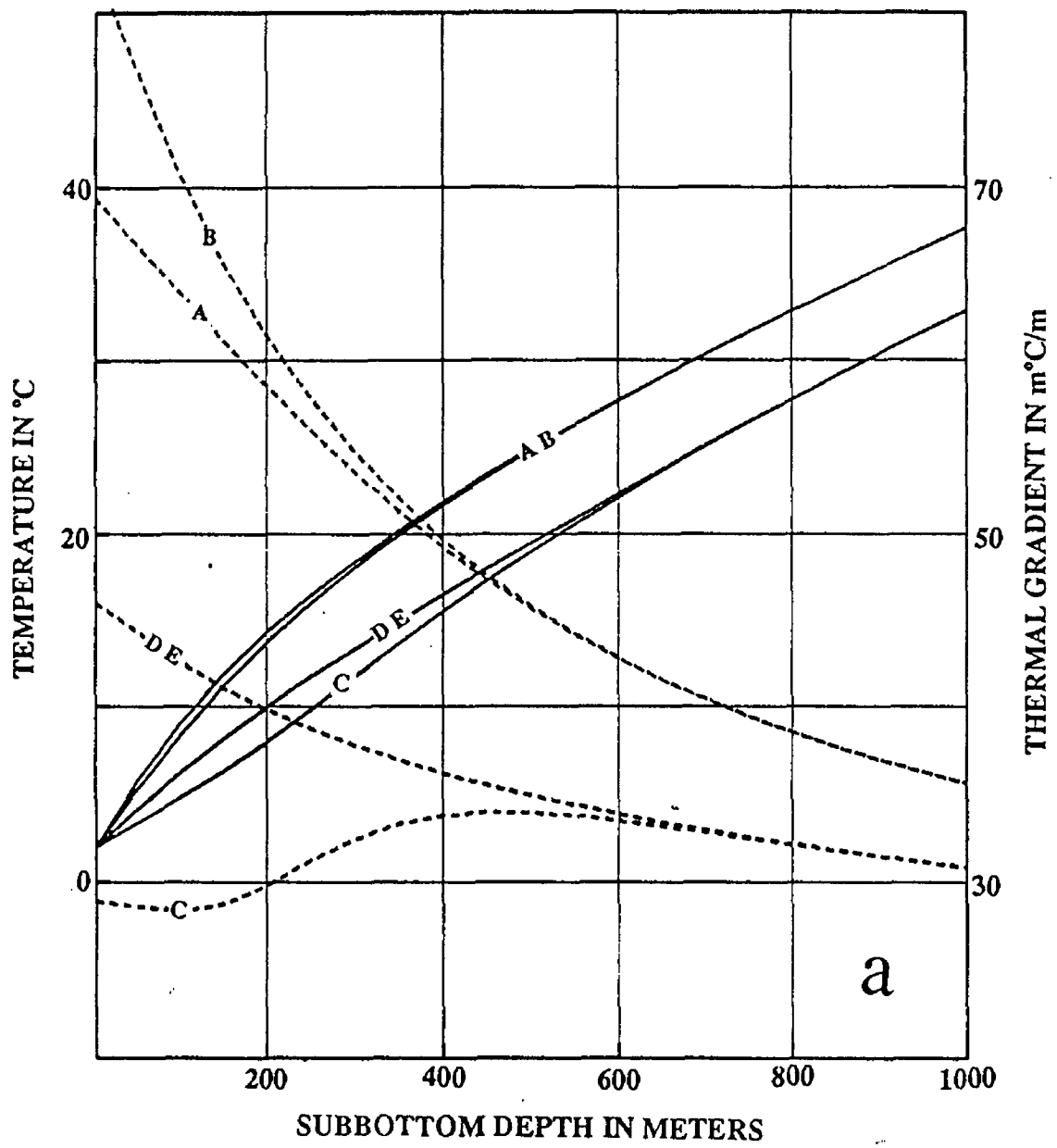


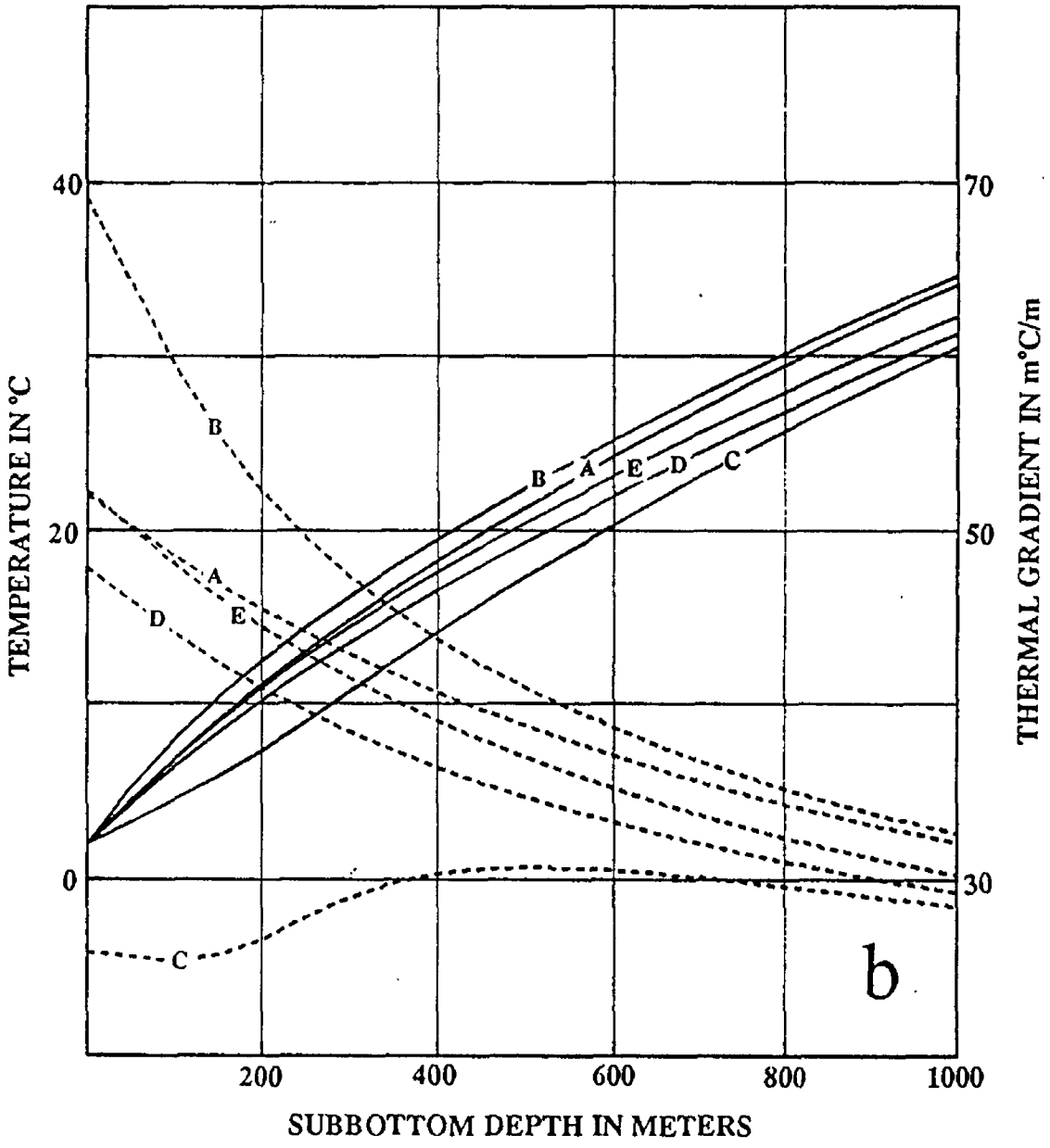


Figure 12. Temperatures (solid lines) and average thermal gradients (dashed lines) at 5 locations (Figure 1) with an advective fluid flow with a magnitude of $-2.0e^{-10}\phi$ *m/s* for the landslide model. Other model parameters are $T_o$ = 2.0°C and Q = 38 mW/m$^2$ (a constant heat flux boundary condition at the depth of 4,000 m). a) At 2,000 years after slide. b) The steady-state condition.

## CONCLUSIONS

In order to predict accurate temperature distribution for a realistic thermal model, which includes thermal conductivity that increases with depth and accommodates a heat source and/or an advective fluid transport, a numerical approach such as a finite difference method is required. A finite difference method is flexible enough to accommodate a variety of differerent thermal models. This study demonstrates that internal heat source models can explain nicely the observed heat flow measurement at DSDP 533 hole and the difference of BSR depths along the recent slide on the Carolina Continental Rise, but solutions are not unique. I speculate that possible heat sources considered in this study are heat generated from the conversion of organic material into biogenic gas in the anaerobic zone in the near surface sediments and heat generated from transforming gas into the hydrate at the level of BSR depth. The following conclusions can be drawn from the numerical model studies.

1) The depth-dependent average thermal gradients at DSDP 533 may be explained by introducing a shallow heat source, but the numerical modeling indicates that the heat source model is not unique.

2) Analyses of BSR depths along a landslide on the Carolina Rise indicate that a thermal model employing a heat source near the current BSR depth within the slide scar area and a shallow heat source (40 m to 140 m) in the adjacent undisturbed area accurately predicts the observed subbottom depths to the BSR across the slide. Because there are no available heat flow data along the seismic profile, the proposed thermal model for the slide is considered highly unconstrained and speculative.

3) The current subbottom depth to the BSR at the slide area is about 430 m, but the model predicts that it will become about 620 m when heat is no longer supplied or hydrate formation no longer occurs at the BSR level and the steady-state condition is reached.

4) A thermal model using advective fluid flow causes the same magnitude of surface heat flow anomaly as the internal heat source, but the observed BSR depths do not fit the modeled results.

## REFERENCES


Carnahan, B., Luther, H.A., and Wilkes, J.O., 1969, Applied Numerical methods: John Wiley & Sons, New York, 604 p.

Davis, E.E., and Hyndman R.D., 1990, Rates of fluid expulsion across the Northern Cascadia accretionary prism from new heat flow and multichannel reflection seismic data: Journal of Geophysical Research, v.95, p. 8869-8889.

Dillon, W.P., and Paull, C.K., 1983, Marine gas hydrate- II: Geophysical evidence, in Cox, J.L., ed., Natural Gas Hydrates: Properties, occurrence and recovery, Butterworth Publishers, Boston, p. 73-90.

Hildebrand, F.S., 1963, Advanced calculus for applications: Prentice-Hall, Englewood Cliffs, New Jersey, 646 p.

Hutchison, Iain, 1985, The effects of sedimentation and compaction on oceanic heat flow: Geophysical Journal of the Royal Astronomical Society, v. 82, p. 439-459.

Kvenvolden, K.A., 1993, A primer on gas hydrates, in Howell, D.G., ed., The future of energy gases: U.S. Geological Survey Professional Paper 1570, p. 279-291.

Lee, M.W., Dillon, W.P., and Hutchinson, D.R., 1992, Estimating the amount of gas hydrates in marine sediments in the Blake Ridge area, Southeastern Atlantic Margin: U.S. Geological Survey Open-File Report 92-275, 24 p.

Lee, M.W., Hutchinson, D.R., Dillon, W.P., Miller, J.J., Agena, W.F., and Swift, B.A., 1993, Method of estimating the amount of in situ gas hydrates in deep marine sediments: Marine and Petroleum Geology., V. 10, p. 493-506.

Macleod, M.K., 1982, Gas hydrates in ocean bottom sediments: The American Association of petroleum Geologists Bulletin, v. 66, p. 2649-2662.

Markl, R.G., Bryan, G.M., and Ewing J.I., 1970, Structure of the Blake-Bahama Outer Ridge: Journal of Geophysical Research, v. 75, p. 4539-4555.

Minshull, T., and White, R., 1989, Sediment compacting and fluid migration in the Makran accretionary prism: Journal of Geophysical Research, v. 94, p. 7387-7402.

Sass, J.H., Lachenbruch, H., and Munroe, R.J., 1971, Thermal conductivity of rocks from measurements on fragments and its application to heat-flow determination: Journal of Geophysical Research, v. 76, p. 3391-3401.

Sawyer, D.S., 1982, Thermal evolution of the northern United States Atlantic continental margin: Ph.D. Thesis, MIT, Cambridge, Massachusetts.

Sclater, J.C., and Francheteau J., 1970, The implications of terrestrial heat flow observations on current tectonic and Geochemical models of the crust and upper mantle of the earth: Geophysical Journal of the Royal Astronomical Society, v. 20, p. 509-542.

Sheridan, R.B., Gradstein, F.M., and others, 1983, Initial reports of the deep sea drilling project , v. 76. p. 35 - 80.

Shipley, T.H., Houston, M.H., Buffler, R.T., Shaub, F.J., McMillen, K.J., Ladd, J.W., and Worzel, J.L, 1979, Seismic evidence for widespread possible gas hydrate horizons on continental slopes and rises: The American Association of Petroleum Geologists Bulletin, v. 63., No. 12, p. 2204-2213.

Sloan, E.D., Jr., 1990, Clathrate Hydrates of natural gases: Mercel Dekker Inc., New York, 641 p.

Tucholke, B.E., Bryan, G.M., and Ewing, J.I., 1977, Gas hydrate horizons detected in seismic-profile data from the western North Atlantic: The American Association of Petroleum Geologists Bulletin, v. 61. p. 698-707.

Uyeda, M.Y.S., Aoki, Y., and Shipley, T.H., 1982, Estimates of heat flow derived from gas hydrates: Geology, v. 10., p. 339-343.

Wachspress, E.L., 1960, The numerical solution of boundary value problems, in Ralston, A. and Wilf, H.S. eds., Mathematical methods for digital computers: New York, John Wiley & Sons, Volume 1, p. 121-127.

## APPENDIX

```
C
C       COMPUTER PROGRAM FOR THE FIGURE 10
C       ARGUMENT DEFINITION
C
C       DX = DZ  : DEPTH SAMPLING INTERVAL IN METER
C       DT       : TIME SAMPLING INTERVAL IN YEAR
C       TMAX     : MAXIMUM TIME FOR THE COMPUTATION
C       ITYPE    : BOUNDARY CODE AT THE LOWER BOUNDARY
C                  1 = CONSTANT TEMPERATURE BOUNDARY CONDITION
C                  2 = CONSTANT FLUX BOUNDARY CONDITION
C       G        : THERMAL FLUX AT THE LOWER BOUNDARY ( mW/(m*m))
C       CD       : COMPACTION CONSTANT IN METER
C       TO       : TEMPERATURE AT THE WATER BOTTOM
C       BOT      : DEPTH WHERE CONSTANT HEAT FLUX IS MAINTAINED
C       AK       : CONDUCTIVITY
C       PHI      : POROSITY
C       H        : SOURCE FUNCTION
C       T, TN    : TEMPERATURE
C       TO       : TEMPERATURE AT THE UPPER SURFACE
C
      DIMENSION T(14400), TN(14400), H(14400)
      DIMENSION PHI(1000), AK(1000), A(1000), B(1000), C(1000)
      COMMON /BK1/G, TO, TL, DX, DZ
      DX= 50.
      DT= 20.
      TMAX= 20001.
      DZ= DX
      NSTEP= IFIX(TMAX / DT) + 1
      JSTEP= NSTEP / 5
      DT= DT * 60 * 24 * 365.
      ITYPE = 2
      G= 38.
      CD= 1500.
      TO= 2.0
      BOT= 4000.
C
C       X - Z LOCATION OF THE SCAR (IH, IZ)
C
      IH= IFIX(1000 / DX)
      IZ= IFIX(200 / DX) + 1
      NX= IFIX(BOT / DX) + 1
      NZ= IFIX(BOT / DX) + 1
      NXX= NX + 2
      N1= 1
      N2= N1 + NXX
      N3= N2 + NXX
      N4= N3 + NXX
      N5= N4 + NXX
      N6= N5 + NXX
      N7= N6 + NXX
C
C       COMPUTATION OF THE VARIABLE CONDUCTIVITY AND SOME PERTINENT VARIABLES
C
      CALL VARK(PHI, AK, CD, NZ, DZ, DT, A, B, C)
C
C       DETERMINE INITIAL CONDITIONS USING ONE-DIMENSIONAL EQUATION
C
      CALL INITIAL(T, AK, TN(N1), TN(N2), TN(N3), TN(N4),
     1     TN(N5), TN(N6), TN(N7), NX, NZ)
C
```

```
C       SOURCE FUNCTION
C
        CALL SOURCE(H, NX, NX, IH, DT)
C
C       ITERATION FOR THE (N+1)-TH STEP FROM THE N-TH STEP
C
        DO  J= 1, NSTEP
        CALL ITER(T, TN, H, PHI, AK, NX, NZ, IH, IZ, DT,  J,
     1   JSTEP, ITYPE, A, B, C)
        END DO
100     FORMAT(4F)
        STOP
        END
C
        SUBROUTINE INITIAL(T, AK, A, B, C, D, E, S, Y, NX, NZ)
        DIMENSION T(NX, NZ), AK(1), A(1), B(1), C(1), D(1), E(1), S(1), Y(1)
        COMMON /BK1/G, TO, TL, DX, DZ
        CALL COEFST(AK, A, B, C, D, NX, 2)
        CALL BUDVAL(A, B, C, D, E, S, Y, NX)
        DO  L = 1, NX
        DO  M= 1, NZ
        T(L, M)= Y(M)
        END DO
        END DO
        TL= T(1, NZ)
        RETURN
        END
C
        SUBROUTINE BUDVAL(A, B, C, D, E, S, Y, NMAX)
        DIMENSION A(1), B(1), C(1), D(1), E(1), S(1), Y(1)
C
C       INITIALIZATION
C
        S(1)= A(1) / B(1)
        E(1)= D(1) / B(1)
        DO  L= 2, NMAX
        TEMP= B(L) - C(L) * S(L-1)
        S(L)= A(L) / TEMP
        E(L)= (D(L) + C(L) * E(L-1)) / TEMP
        END DO
C
C       OUTPUT
C
        Y(NMAX)= E(NMAX)
        DO  L= NMAX - 1, 1, -1
        Y(L)= S(L) * Y(L + 1) + E(L)
        END DO
        RETURN
        END
C
        SUBROUTINE VARK(PHI, AK, CD, NMAX, DZ, DT, A, B, C)
        DIMENSION PHI(1), AK(1), A(1), B(1), C(1)
        BETA= 0.25E07
        BETAO= 1.0E07
        AKR= 2.4
        AKW= 0.6
        DX= DZ
        PHIO= 0.65
        CON1= DT / (BETA * DX * DX)
        CON3= DT * BETAO /(2 * DX * BETA)
        CON4= DT * BETAO /(2 * DZ * BETA)
        CON5= DT / BETA
        DO  M= 1, NMAX
```

```
      DIST= (M - 1) * DZ
      POR= PHIO * EXP(- DIST/CD)
      AK(M)= AKW ** POR * AKR ** (1.0 - POR)
      CONST= EXP(-DIST/300.)
      CONST= 1.0
      PHI(M)= -2.0E-10 * CONST * POR * CON3
      END DO
      CON= DT /(4 * BETA * DX * DX)
      DO  M= 1, NMAX
      A(M)= AK(M+1) + 4.0 * AK(M) - AK(M-1)
      B(M)= - AK(M+1) + 4.0 * AK(M) + AK(M -1)
      C(M)= - 8 * AK(M)
      A(M)= CON * A(M)
      B(M)= CON * B(M)
      C(M)= CON * C(M)
      END DO
      RETURN
      END
C
      SUBROUTINE SOURCE(H, NX, NZ, IH, DT)
      DIMENSION H(NX, NZ)
      BETA= 0.25E07
      CON5= DT / BETA
      DO  I= IH, NX
      DO  N= 2, 3
      H(I, N)= CON5 * 0.01 / 150.
      END DO
      END DO
      DO  I= 1, IH
      DO  J = 14,15
      H(I, J)= CON5 * 0.03 / 100.
      END DO
      END DO
      RETURN
      END
C
      SUBROUTINE ITER(T, TN, H, PHI, AK, NX, NZ, IH, IZ, DT,
     1  ISTEP, JSTEP, ITYPE, A, B, C)
      DIMENSION T(NX, NZ), TN(NX, NZ), H(NX, NZ)
      DIMENSION PHI(NZ), AK(NZ), A(1), B(1), C(1)
      COMMON /BK1/ G, TO, TL, DX, DZ
      LOGICAL VIRGIN
      DATA VIRGIN /.TRUE./
      IF(VIRGIN) THEN
      VIRGIN= .FALSE.
      QB= G/1000.
      BETA= 0.25E07
      BETAO= 1.0E07
      DZ= DX
      IOUT2= IFIX(900/DX) + 1
      IOUT3= IFIX(1100/DX) + 1
      IOUT4= IFIX(1600/DX) + 1
      CON1= DT / (BETA * DX * DX)
      CON3= DT * BETAO /(2 * DX * BETA)
      CON4= DT * BETAO /(2 * DZ * BETA)
      CON5= DT / BETA
      DELT= QB * DZ / AK(NZ)
      DO  M= 1, NZ
      AK(M)= AK(M) * CON1
      END DO
      END IF
      DO  I = 2, IH
      DO  J= IZ + 1, NZ - 1
```

```
      T1= AK(J) * ( T(I+1, J) - T(I, J) - T(I,J) + T(I-1, J))
      T2= A(J) * T(I, J+1) + C(J) * T(I,J) + B(J) * T(I, J -1)
      T3= PHI(J+1) * T(I, J+1) - PHI(J-1) * T(I, J-1)
      TN(I,J)= T1 + T2 - T3 + H(I, J) + T(I, J)
      END DO
      END DO
      DO  I = IH + 1, NX - 1
      DO  J = 2, NZ - 1
      T1= AK(J) * (T(I+1, J) - T(I,J) - T(I,J) + T(I-1, J))
      T2= A(J) * T(I, J+1) + C(J) * T(I,J) + B(J) * T(I, J -1)
      T3= PHI(J+1) * T(I, J+1) - PHI(J-1) * T(I, J-1)
      TN(I,J)= T1 + T2 - T3 + H(I, J) + T(I, J)
      END DO
      END DO
C
C     BOUNDARY CONDITION
C
      DO  I = 1, NX
      TN(I, 1) = TO
      TN(I, NZ)= TN(I, NZ - 1) + DELT
      END DO
      DO  I= 1, IH
      DO  J= 1, IZ
      TN(I, J)= TO
      END DO
      END DO
      DO  J= 1, NZ
      TN(1, J)= TN(2, J)
      TN(NX, J) = TN(NX -1, J)
      END DO
      DO  I= 1, NX
      DO  J= 1, NZ
      T(I, J)= TN(I, J)
      END DO
      END DO
      IF(MOD(ISTEP, JSTEP) .EQ. 1) THEN
      WRITE(60,100)(T(1, J), J = IZ, NZ)
      WRITE(60,100)(T(IOUT2,J), J = IZ, NZ)
      WRITE(60,100)(T(IOUT3,J), J = 1, NZ-IZ + 1)
      WRITE(60,100)(T(IOUT4,J), J = 1, NZ-IZ + 1)
      WRITE(60,100)(T(NX-1, J), J = 1, NZ-IZ + 1)
100   FORMAT(4F)
      END IF
      RETURN
      END
C
      SUBROUTINE COEFST(AK, A, B, C, D, NMAX, ITYPE)
      DIMENSION AK(1), A(1), B(1), C(1), D(1)
      COMMON /BK1/G, TO, TL, DX, DZ
      DZ2= 0.25 / (DZ * DZ)
      DO  M=  2, NMAX - 1
      A(M)= -(AK(M+1) - AK(M -1) + 4*AK(M)) * DZ2
      B(M)= -8.0 * AK(M) * DZ2
      C(M)= -(-AK(M + 1) + 4* AK(M) + AK(M-1)) * DZ2
      END DO
      A(1)= 0.
      C(NMAX)= 0.
      A(NMAX)= 0.
      C(1)= 0.
      B(1)= 1.0
      B(NMAX)= 1.0
C
C     BOUNDARY CONDITION
```

```
C
      D(1)= TO
      IF(ITYPE .EQ. 1) THEN
      D(NMAX)= TL
      C(NMAX)= 0.0
      ELSE
      D(NMAX)= G * DZ / (1000 * AK(NMAX))
      C(NMAX)= 1.
      END IF
      RETURN
      END
```